JACS
JOURNAL OF THE AMERICAN CHEMICAL SOCIETY

Communication

pubs.acs.org/JACS

Metal–Organic Frameworks with Precisely Designed Interior for Carbon Dioxide Capture in the Presence of Water

Alejandro M. Fracaroli,[†] Hiroyasu Furukawa,[†] Mitsuharu Suzuki,[†] Matthew Dodd,[§] Satoshi Okajima,[†] Felipe Gándara,[†] Jeffrey A. Reimer,[§] and Omar M. Yaghi*[,†,‡]

[†]Department of Chemistry, University of California—Berkeley, Materials Sciences Division, Lawrence Berkeley National Laboratory, and Kavli Energy NanoSciences Institute at Berkeley, Berkeley, California 94720, United States

[‡]King Fahd University of Petroleum and Minerals, Dhahran 34464, Saudi Arabia

[§]Department of Chemical and Biomolecular Engineering, University of California—Berkeley, and Environmental Energy Technologies Division, Lawrence Berkeley National Laboratory, Berkeley, California 94720, United States

Supporting Information

ABSTRACT: The selective capture of carbon dioxide in the presence of water is an outstanding challenge. Here, we show that the interior of IRMOF-74-III can be covalently functionalized with primary amine (IRMOF-74-III-CH_2NH_2) and used for the selective capture of CO_2 in 65% relative humidity. This study encompasses the synthesis, structural characterization, gas adsorption, and CO_2 capture properties of variously functionalized IRMOF-74-III compounds (IRMOF-74-III-CH_3, -NH_2, -CH_2NHBoc, -$CH_2NMeBoc$, -CH_2NH_2, and -CH_2NHMe). Cross-polarization magic angle spinning ^{13}C NMR spectra showed that CO_2 binds chemically to IRMOF-74-III-CH_2NH_2 and -CH_2NHMe to make carbamic species. Carbon dioxide isotherms and breakthrough experiments show that IRMOF-74-III-CH_2NH_2 is especially efficient at taking up CO_2 (3.2 mmol of CO_2 per gram at 800 Torr) and, more significantly, removing CO_2 from wet nitrogen gas streams with breakthrough time of 610 ± 10 s g^{-1} and full preservation of the IRMOF structure.

Carbon dioxide capture from combustion sources such as flue gas in power plants is an outstanding challenge because CO_2 has to be selectively removed from other gases and, most importantly, water.[1] Porous materials can trap CO_2 in voluminous amounts, but when water is present the efficiency of capture is significantly reduced, as water competes for the binding sites within the pores.[2] Aqueous monoethanolamine (MEA) solutions are efficient at binding CO_2; however, they present a major energy cost and environmental hazard.[3] Thus, a need exists to develop materials capable of addressing this carbon capture challenge.

The preferred method for measuring the efficiency of a given material for capture of CO_2 is to expose a solid form of the material to a mixture of gases containing CO_2 and water, and then to detect the gases and measure the time they take to pass through the material (breakthrough time).[4] Various porous materials[5] such as zeolites, mesoporous silica, polymeric resins, porous carbon, and metal–organic frameworks (MOFs) are being studied for their CO_2 capture properties, but a viable class of materials for this application has yet to emerge. Although carbon capture in mesoporous materials and carbon has been shown under humid conditions,[4c] MOFs show special promise because of their adjustable chemical functionality, structural diversity, and ease of functionalization.[6] Capture of CO_2 from dry gas mixtures (nitrogen, methane, and oxygen) has been reported in MOFs incorporating amines bound to either metal sites[7] or organic linkers.[8] However, successful demonstrations of MOFs capable of CO_2 capture in the presence of water, and doing so without degradation of performance as a result of competition with water, remain uncommon.[4b]

In this Communication, we show how the interior of porous MOFs can be designed to overcome the complications presented by the competition of water with CO_2. We chose a MOF constructed from magnesium oxide rods joined by terphenylene organic linkers {IRMOF-74-III, Mg_2(DH3PhDC), where H_4DH3PhDC = 2′,5′-dimethyl-3,3″-dihydroxy-[1,1′:4′,1″-terphenyl]-4,4″-dicarboxylic acid, Figure 1} to make an extended structure with an **etb** topology supporting one-dimensional channels of 25 Å in their diagonal.[9] The organic linkers and their corresponding IRMOF-74-III structures were functionalized with -CH_3, -NH_2, -CH_2NHBoc, -$CH_2NMeBoc$, -CH_2NH_2, and -CH_2NHMe (Boc = *tert*-butyloxycarbonyl), which point toward the center of the channels (Figure 1). Here, we report the synthesis, characterization, porosity, and CO_2 capture properties (in dry and wet nitrogen streams) of IRMOF-74-III with the six different functionalities, *vide supra*. We find that at low pressure IRMOF-74-III-CH_2NH_2 and -CH_2NHMe exhibit strong binding of CO_2 and have the highest uptake, and that in breakthrough experiments the -CH_2NH_2 form shows selectivity toward CO_2 in a wet nitrogen gas stream with 65% relative humidity (RH). Indeed, the behavior of this material under wet conditions remains unchanged from that observed under dry gas stream.

The synthesis of the appropriate linkers for IRMOF-74-III compounds is shown in Figure 1. Starting from the commercially available methyl 2-hydroxy-4-iodobenzoate (**1**),

Received: April 2, 2014
Published: June 9, 2014

   dx.doi.org/10.1021/ja503296c | *J. Am. Chem. Soc.* 2014, 136, 8863–8866

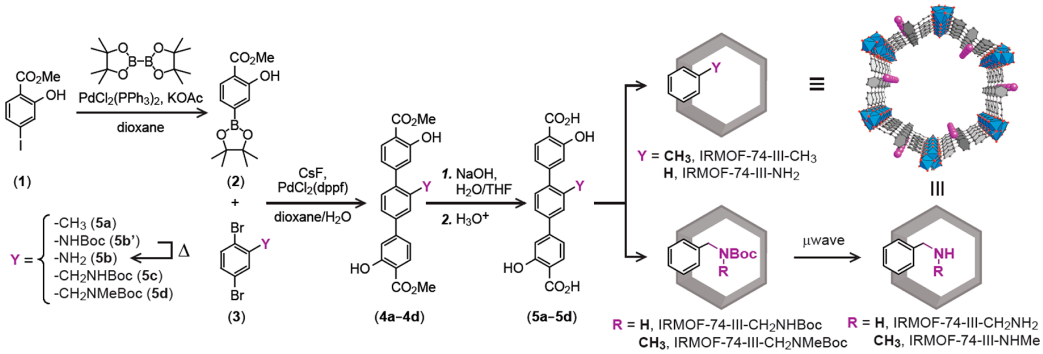

Figure 1. Synthetic pathway for the functionalized organic linkers used in the synthesis of IRMOF-74-III. This methodology allowed us to prepare -CH_3 (**5a**), -NH_2, (**5b**), -CH_2NHBoc (**5c**), and -$CH_2NMeBoc$ (**5d**) functionalized linkers. On the right is shown a schematic representation of the IRMOF-74-III pore as functionalized with the organic linkers **5a**–**5d** and post-synthetic deprotection of Boc groups. Color code: C in gray, O in red, functional groups in purple, Mg as blue polyhedra.

we synthesized four different organic linkers by using Suzuki–Miyaura coupling of boronic acid pinacol ester (**2**) and functionalized 1,4-dibromobenzenes (**3**), followed by saponification reaction of the methyl ester linker derivatives (**4a**–**4d**). The synthetic method was designed to achieve versatility in the covalent incorporation of a variety of functional groups within the pores of IRMOF-74-III. The linkers **5a**–**5d** have -CH_3, -NH_2, -CH_2NHBoc, and -$CH_2NMeBoc$ functional groups, respectively. We have employed the Boc protecting group in order to introduce -CH_2NH_2 and -CH_2NHMe into IRMOF-74-III, as the unprotected amines may react with the metal ions used for the MOF structure synthesis. The synthesized linkers were fully characterized by nuclear magnetic resonance (^1H and ^{13}C NMR) and electrospray ionization mass spectrometry (ESI-MS), and single-crystal X-ray diffraction (XRD) in the case of -NH_2 and -$CH_2NMeBoc$ linkers [section S1, Supporting Information (SI)].

Four IRMOF-74-III structures incorporating **5a**–**5d** were prepared according to reported conditions.[9] The synthesis of IRMOF-74-III-CH_2NHBoc is typical: a solvent mixture containing $Mg(NO_3)_2{\cdot}6H_2O$ (160 mg, 0.62 mmol), linker **5c** (90 mg, 0.19 mmol), and 15 mL of *N*,*N*-dimethylformamide (DMF)/ethanol/water (9:0.5:0.5) was placed in a 20 mL capped vial, which was heated at 120 °C for 20 h. Depending on the functionality incorporated in the interior of the MOF, white (-CH_3), yellow (-NH_2), or pale yellow (-CH_2NHBoc and -$CH_2NMeBoc$) microcrystalline solids were obtained (Figure S3).

The Boc protecting groups in IRMOF-74-III-CH_2NHBoc and -$CH_2NMeBoc$ were removed using a modification of a reported post-synthetic deprotection procedure.[10] In our case, microwave heating was applied (230 °C) for 10 min in a ternary mixture of solvents [2-ethyl-1-hexanol/ethylene glycol/water (9.1:0.5:0.5)]. This process allowed us to quantitatively obtain the unprotected primary (-CH_2NH_2) and secondary amine (-CH_2NHMe) groups in the interior of those MOFs. The successful deprotection was examined by solution ^1H NMR spectra of the digested samples in 50 mM DCl in a DMSO-d_6/D_2O mixture, where the absence of the corresponding Boc group resonance peaks at δ = 1.35 ppm and δ = 1.28 ppm was confirmed for IRMOF-74-III-CH_2NH_2 and -CH_2NHMe, respectively. Similar NMR analysis was carried out for the remaining IRMOF-74-III structures and confirmed the presence of the appropriate functionality (section S4, SI).

To evaluate the porosity and crystallinity of these materials, as-synthesized samples were activated by immersion in 10 mL of DMF for 4 h, the liquid was decanted, and then the process was repeated three times per day for 3 days. This whole protocol was repeated with methanol during 3 additional days to obtain the solid with washed interior. The solvent within the pores of the resulting solids was removed under dynamic vacuum initially at room temperature and then by heating at 120 °C for 12 h. The crystallinity and structure of the evacuated series of IRMOF-74-III compounds were confirmed by the coincidence of the sharp powder X-ray diffraction (PXRD) lines with those of the parent unfunctionalized IRMOF-74-III (section S5, SI). In addition, PXRD analysis of the IRMOF-74-III-CH_2NH_2 and -CH_2NHMe samples further confirmed that the frameworks maintain their structural integrity and porosity after post-synthetic deprotection of the Boc groups. Nitrogen adsorption isotherms were measured at 77 K, and the Brunauer–Emmett–Teller (BET) surface areas were calculated to be 2640, 2720, 2170, 2220, 2310, and 2250 $m^2\ g^{-1}$ for IRMOF-74-III-CH_3, -NH_2, -CH_2NHBoc, -$CH_2NMeBoc$, -CH_2NH_2, and -CH_2NHMe, respectively. These values are similar to the BET surface area of the parent IRMOF-74-III (2440 $m^2\ g^{-1}$),[9] indicating that porosity is maintained in the functionalized as well as the deprotected forms.

The CO_2 uptake capacity for each of the functionalized IRMOF-74-III compounds was obtained by measuring the corresponding isotherms at 25 °C (Figure 2a). All the compounds showed significant CO_2 uptake, and, as expected, IRMOF-74-III-CH_3, -NH_2, -CH_2NH_2, and -CH_2NHMe exhibit similar capacity at 800 Torr, while the protected compounds IRMOF-74-III-CH_2NHBoc and -$CH_2NMeBoc$ showed lesser uptake because of the sterically bulky Boc groups (Figure 2a). Interestingly, IRMOF-74-III-CH_2NH_2 and -CH_2NHMe showed the highest uptake capacities at low CO_2 pressure range (<1 Torr, Figure 2b) with hysteresis, retaining ca. 20 $cm^3\ g^{-1}$ of CO_2 upon desorption down to 10 Torr (Figure 2a). This trend can be attributed to the strong interactions between CO_2 and aliphatic amine functionalities. A second CO_2 isotherm was recorded after evacuation of the sample at room temperature for 2 h (second cycle, Figure 2c). As expected, the initial slope of the CO_2 uptake in the second cycle for IRMOF-74-III-CH_2NH_2 and -CH_2NHMe was 1/3.6 and 1/4.6 compared to the first cycle, and the maximum uptakes at 800 Torr were less than those of the first cycles (by ca. 18 and 15 $cm^3\ g^{-1}$ for

dx.doi.org/10.1021/ja503296c | J. Am. Chem. Soc. 2014, 136, 8863–8866

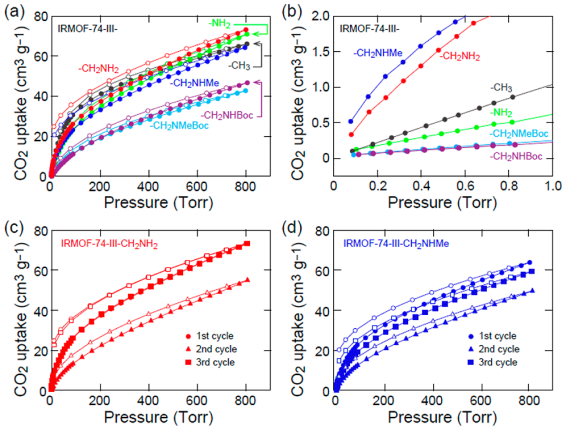

Figure 2. (a) Comparison of CO_2 uptake at 25 °C for IRMOF-74-III-CH_3 (gray), -NH_2 (green), CH_2NH_2 (red), -CH_2NHMe (blue), -CH_2NHBoc (purple), and -CH_2NMeBoc (cyan). (b) Expansion of the low pressure range (>1 Torr). Carbon dioxide isotherms at 25 °C for IRMOF-74-III-CH_2NH_2 (c) and -CH_2NHMe (d). Uptakes for samples after activation (first cycle), after first CO_2 uptake (second cycle), and after 120 °C heating for 1 h for regeneration (third cycle) are shown in circles, triangles, and squares, respectively.

IRMOF-74-III-CH_2NH_2 and -CH_2NHMe, respectively). As this evidence clearly indicated a strongly bound CO_2, the solids were heated to 120 °C under vacuum (10 mTorr) for 1 h, and isotherms for the third cycle of CO_2 uptake were measured. In the case of IRMOF-74-III-CH_2NH_2, the CO_2 was fully desorbed, while partial desorption was observed for IRMOF-74-III-CH_2NHMe (third cycle, Figure 2c,d).

Cross-polarization magic angle spinning ^{13}C NMR spectra were collected for each of IRMOF-74-III-NH_2, -CH_2NHBoc, -CH_2NH_2, and -CH_2NHMe to evaluate the possibility of carbamate formation, which would be expected in the reaction of CO_2 with IRMOF-74-III-CH_2NH_2 and -CH_2NHMe and not the others. Activated samples of these MOFs were exposed to ^{13}C-labeled CO_2 at room temperature and ca. 760 Torr for 24 h before the samples were transferred into a solid-state NMR rotor. The ^{13}C NMR spectra of IRMOF-74-III-CH_2NH_2 and -CH_2NHMe show a broad resonance peak centered at δ = 160 ppm, corresponding to the chemical shift of carbamate species resonance (carbamate ions and carbamic acid) reported in the literature,[4a,11] while in the case of IRMOF-74-III-NH_2 and -CH_2NHBoc samples, this peak is absent (Figure S18). This difference in the ^{13}C NMR spectra confirms that CO_2 is only chemisorbed by -CH_2NH_2 and -CH_2NHMe amine-functionalized IRMOF-74-III, but not by MOFs with -NH_2 and -CH_2NHBoc functionalities.

Given the fully reversible nature of the CO_2 uptake of IRMOF-74-III-CH_2NH_2 (Figure 2c), we carried out a dynamic separation experiment to evaluate the breakthrough time in the absence and presence of water. Here, a solid sample of IRMOF-74-III-CH_2NH_2 compound (238 mg, 0.56 mmol) was packed in a 10 cm length × 0.6 cm diameter stainless steel column and utilized as an adsorbent bed. A mixed gas containing 16% (v/v) of CO_2 in a nitrogen gas stream was introduced to the column, and the effluent was monitored by a mass spectrometer.[4] The breakthrough time was determined when the CO_2 concentration in the effluent reached 5% of the influent concentration.

Under dry conditions, the IRMOF-74-III-CH_2NH_2 adsorbent bed held CO_2 up to 670 ± 10 s g^{-1}, which is equivalent to a kinetic CO_2 adsorption capacity of 0.8 mmol g^{-1}. The CO_2 influent was then stopped and, to regenerate the material, we purged the adsorbent bed with dry nitrogen; however, this was not enough to fully remove adsorbed CO_2 (Figure 3a). Therefore, the sample bed was heated at 95 °C under nitrogen flow for 30 min, upon which appearance of CO_2 signal on the mass spectrometer indicated the liberation of chemically bound CO_2. The amount of released CO_2 was calculated by integration of the peak area and found to be 50% of the total uptake capacity of the MOF under these conditions. The regenerated IRMOF-74-III-CH_2NH_2 showed a breakthrough time as long as the one for the first run (Figure S19). This indicates that amine functionalities incorporated into the IRMOF-74-III require moderate regeneration conditions compared to MEA (ca. 120 °C) and other amine-functionalized MOFs.[7a] As a control experiment, we subjected IRMOF-74-III-CH_3 under the same conditions used for IRMOF-74-III-CH_2NH_2 and found a longer breakthrough time (1380 ± 10 s g^{-1});[12] however, upon purging the sample with nitrogen, all adsorbed CO_2 was recovered, indicating, as expected, no carbamate formation (Figure S20).

Both IRMOF-74-III-CH_2NH_2 and -CH_3 were examined by similar breakthrough experiments, but now in the presence of water. Prior to the breakthrough measurements, wet nitrogen with 65% RH was introduced to the adsorbent bed until the water concentration of the effluent showed a constant value (>16 h). To estimate the breakthrough time in the presence of water, we introduced a gas mixture containing 16% of dry CO_2

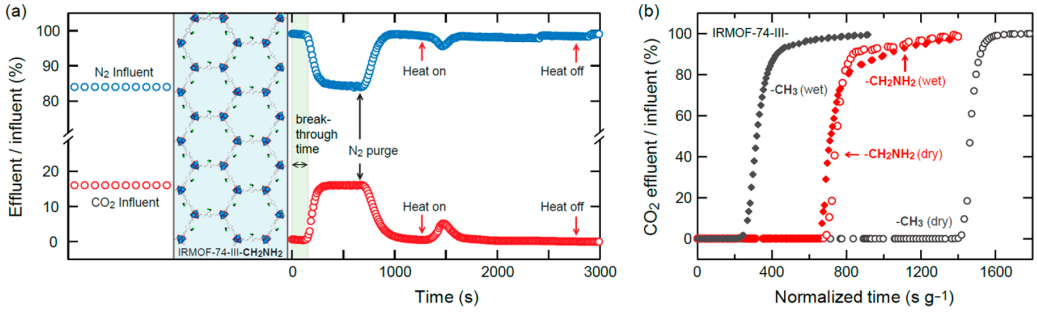

Figure 3. (a) IRMOF-74-III-CH_2NH_2 breakthrough cycle under dry conditions. Breakthrough time is highlighted in light blue. (b) Breakthrough curves for IRMOF-74-III-CH_3 under dry conditions (gray empty markers) and wet conditions (gray filled markers), and for IRMOF-74-III-CH_2NH_2 under dry conditions (red empty markers) and in the presence of water (red filled markers).

dx.doi.org/10.1021/ja503296c | J. Am. Chem. Soc. 2014, 136, 8863−8866

and 84% of wet nitrogen (65% RH). IRMOF-74-III-CH_2NH_2 showed a breakthrough time nearly identical to that observed under dry conditions (610 ± 10 s g^{-1}) (Figure 3b), while the breakthrough time of IRMOF-74-III-CH_3 under wet conditions showed an 80% decrease compared to that in the absence of moisture. This behavior indicates that the CO_2 uptake in IRMOF-74-III-CH_3 is, as expected, mainly attributable to the open magnesium sites, which are occupied by water molecules under humid conditions.[12] In IRMOF-74-III-CH_2NH_2, the CO_2 uptake takes place at the linker amine sites, while the open magnesium sites are not accessible under dry nor humid conditions (section S7, SI); therefore, the effect of water on the CO_2 uptake should be negligible. This is also supported by the dissimilar desorption behavior compared to IRMOF-74-III-CH_3 (Figures 3a and S20).

IRMOF-74-III-CH_2NH_2 with bound CO_2 was regenerated by purging with dry nitrogen followed by heating at 90 °C to remove the CO_2. A second cycle of humidification and CO_2 uptake was applied as explained above to obtain a nearly identical breakthrough time (600 ± 10 s g^{-1}) (section S9, SI). We further note that the PXRD pattern of the sample after these cycles was identical to that of the activated sample, thus indicating full preservation of IRMOF-74-III-CH_2NH_2 structure throughout the CO_2 capture process (Figure S16).

■ ASSOCIATED CONTENT

Supporting Information

Detailed organic linkers and MOFs synthetic procedures, including characterization by NMR spectra, PXRD, nitrogen adsorption, breakthrough experiments, and complete refs 4b, 5g, and 9. This material is available free of charge via the Internet at http://pubs.acs.org.

■ AUTHOR INFORMATION

Corresponding Author

yaghi@berkeley.edu

Notes

The authors declare no competing financial interest.

■ ACKNOWLEDGMENTS

This work was partially supported for synthesis and characterization by BASF SE (Ludwigshafen, Germany), gas adsorption by U.S. Department of Defense, Defense Threat Reduction Agency (HDTRA 1-12-1-0053), and carbon dioxide adsorption studies by the U.S. Department of Energy, Office of Science, Office of Basic Energy Sciences, Energy Frontier Research Center (DE-SC0001015).

■ REFERENCES

(1) Granite, E. J.; Pennline, H. W. *Ind. Eng. Chem. Res.* **2002**, *41*, 5470.

(2) (a) Li, G.; Xiao, P.; Webley, P.; Zhang, J.; Singh, R.; Marshall, M. *Adsorption* **2008**, *14*, 415. (b) Liu, J.; Thallapally, P. K.; McGrail, B. P.; Brown, D. R.; Liu, J. *Chem. Soc. Rev.* **2012**, *41*, 2308. (c) Yu, J.; Balbuena, P. B. *J. Phys. Chem. C* **2013**, *117*, 3383.

(3) (a) Sharma, S. D.; Azzi, M. *Fuel* **2014**, *121*, 178. (b) Gouedard, C.; Picq, D.; Launay, F.; Carrette, P.-L. *Int. J. Greenhouse Gas Control* **2012**, *10*, 244. (c) Johnson, J. *Chem. Eng. News* **2004**, *82* (51, Dec 21), 36.

(4) (a) Li, D.; Furukawa, H.; Deng, H.; Liu, C.; Yaghi, O. M.; Eisenberg, D. S. *Proc. Natl. Acad. Sci. U.S.A.* **2014**, *111*, 191. (b) Nugent, P.; et al. *Nature* **2013**, *495*, 80. (c) Hao, G.-P.; Li, W.-C.; Qian, D.; Wang, G.-H.; Zhang, W.-P.; Zhang, T.; Wang, A.-Q.; Schüth, F.; Bongard, H.-J.; Lu, A.-H. *J. Am. Chem. Soc.* **2011**, *133*, 11378.

(5) (a) Sumida, K.; Rogow, D. L.; Mason, J. A.; McDonald, T. M.; Bloch, E. D.; Herm, Z. R.; Bae, T.-H.; Long, J. R. *Chem. Rev.* **2012**, *112*, 724. (b) Gassensmith, J. J.; Furukawa, H.; Smaldone, R. A.; Forgan, R. S.; Botros, Y. Y.; Yaghi, O. M.; Stoddart, J. F. *J. Am. Chem. Soc.* **2011**, *133*, 15312. (c) Britt, D.; Furukawa, H.; Wang, B.; Glover, T. G.; Yaghi, O. M. *Proc. Natl. Acad. Sci. U.S.A.* **2009**, *106*, 20637. (d) Horike, S.; Kishida, K.; Watanabe, Y.; Inubushi, Y.; Umeyama, D.; Sugimoto, M.; Fukushima, T.; Inukai, M.; Kitagawa, S. *J. Am. Chem. Soc.* **2012**, *134*, 9852. (e) Xiang, S.; He, Y.; Zhang, Z.; Wu, H.; Zhou, W.; Krishna, R.; Chen, B. *Nat. Commun.* **2012**, *3*, 954. (f) Li, T.; Sullivan, J. E.; Rosi, N. L. *J. Am. Chem. Soc.* **2013**, *135*, 9984. (g) Li, B.; et al. *Angew. Chem., Int. Ed.* **2012**, *51*, 1412. (h) Wriedt, M.; Sculley, J. P.; Yakovenko, A. A.; Ma, Y.; Halder, G. J.; Balbuena, P. B.; Zhou, H.-C. *Angew. Chem., Int. Ed.* **2012**, *51*, 9804. (i) Deria, P.; Mondloch, J. E.; Tylianakis, E.; Ghosh, P.; Bury, W.; Snurr, R. Q.; Hupp, J. T.; Farha, O. K. *J. Am. Chem. Soc.* **2013**, *135*, 16801. (j) Lu, A.-H.; Hao, G.-P. *Annu. Rep. Prog. Chem., Sect. A: Inorg. Chem.* **2013**, *109*, 484. (k) Hedin, N.; Andersson, L.; Bergstrom, L.; Yan, J. *Appl. Energy* **2013**, *104*, 418. (l) Samanta, A.; Zhao, A.; Shimizu, G. K. H.; Sarkar, P.; Gupta, R. *Ind. Eng. Chem. Res.* **2012**, *51*, 1438.

(6) (a) Furukawa, H.; Cordova, K. E.; O'Keeffe, M.; Yaghi, O. M. *Science* **2013**, *341*, 974. (b) Furukawa, H.; Cordova, K. E.; O'Keeffe, M.; Yaghi, O. M. *Science* **2013**, *341*, 1230444.

(7) (a) McDonald, T. M.; Lee, W. R.; Mason, J. A.; Wiers, B. M.; Hong, C. S.; Long, J. R. *J. Am. Chem. Soc.* **2012**, *134*, 7056. (b) Planas, N.; Dzubak, A. L.; Poloni, R.; Lin, L.-C.; McManus, A.; McDonald, T. M.; Neaton, J. B.; Long, J. R.; Smit, B.; Gagliardi, L. *J. Am. Chem. Soc.* **2013**, *135*, 7402. (c) Lee, W. R.; Hwang, S. Y.; Ryu, D. W.; Lim, K. S.; Han, S. S.; Moon, D.; Choi, J.; Hong, C. S. *Energy Environ. Sci.* **2014**, *7*, 744. (d) Cao, Y.; Song, F.; Zhao, Y.; Zhong, Q. *J. Environ. Sci.* **2013**, *25*, 2081. (e) Demessence, A.; D'Alessandro, D. M.; Foo, M. L.; Long, J. R. *J. Am. Chem. Soc.* **2009**, *131*, 8784.

(8) (a) Lu, W.; Sculley, J. P.; Yuan, D.; Krishna, R.; Wei, Z.; Zhou, H.-C. *Angew. Chem., Int. Ed.* **2012**, *51*, 7480. (b) Arstad, B.; Fjellvåg, H.; Kongshaug, K. O.; Swang, O.; Blom, R. *Adsorption* **2008**, *14*, 755. (c) Qiao, Z.; Zhou, J.; Lu, X. *Fluid Phase Equilib.* **2014**, *362*, 342.

(9) Deng, H.; et al. *Science* **2012**, *336*, 1018.

(10) (a) Cohen, S. M. *Chem. Rev.* **2012**, *112*, 970. (b) Lun, D. J.; Waterhouse, G. I. N.; Telfer, S. G. *J. Am. Chem. Soc.* **2011**, *133*, 5806.

(11) Pinto, M. L.; Mafra, L.; Guil, J. M.; Pires, J.; Rocha, J. *Chem. Mater.* **2011**, *23*, 1387.

(12) Liu, J.; Benin, A. I.; Furtado, A. M. B.; Jakubczak, P.; Willis, R. R.; LeVan, M. D. *Langmuir* **2011**, *27*, 11451.

Supporting Information (48 pages) for

Metal-Organic Frameworks with Precisely Designed Interior for Carbon Dioxide Capture in the Presence of Water

Alejandro M. Fracaroli,[†] Hiroyasu Furukawa,[†] Mitsuharu Suzuki,[†] Matthew Dodd,[§] Satoshi Okajima,[†] Felipe Gándara,[†] Jeffrey A. Reimer[§] and Omar M. Yaghi*[,†,‡]

[†] Department of Chemistry, University of California - Berkeley, Materials Sciences Division, Lawrence Berkeley National Laboratory, and Kavli Energy NanoSciences Institute at Berkeley, Berkeley, California 94720, United States

[‡] King Fahd University of Petroleum and Minerals, Dhahran 34464, Saudi Arabia

[§] Department of Chemical and Biomolecular Engineering, University of California - Berkeley, and Environmental Energy Technologies Division, Lawrence Berkeley National Laboratory, Berkeley, California 94720, United States

Table of Contents

1. Synthesis of organic linkers

1.1. General

All reactions were carried out under nitrogen unless otherwise noted. Tetrahydrofuran (THF) and dichloromethane (CH_2Cl_2) were treated with a Grubbs-type apparatus prior to use. Anhydrous *N*,*N*-dimethylformamide (DMF), and methanol were obtained from EMD Millipore Chemicals. Other solvents and reagents were obtained from commercial sources and used without further purification. ^{1}H and $^{13}C\{^{1}H\}$ NMR spectra were acquired on a Bruker ARX-500 (500 MHz), DRX-500 (500 MHz), or AVB-400 (400 MHz) spectrometer at 297–300 K, and chemical shifts were calculated using the solvent resonances as internal standards (^{1}H: 7.26 ppm for $CHCl_3$, 2.05 ppm for acetone-d_6, 2.50 ppm for DMSO;$^{13}C\{^{1}H\}$: 77.00 ppm for $CDCl_3$, 29.84 ppm for acetone-d_6, 39.51 ppm for DMSO-d_6). Infrared spectra were recorded on a Bruker ALPHA Platinum ATR-FTIR Spectrometer equipped with a single reflection diamond ATR module, and wavenumbers are reported in cm^{-1} with peak descriptions: s (strong), m (medium), w (weak), br (broad), sh (shoulder). High Resolution Electrospray Ionization mass (HR-ESI) was acquired on an Finnigan LTQ FT (Thermo Electron Corporation) instrument, using negative mode and by direct injection of methanol solutions of the samples using syringe pump with a flow rate of 5 μL min^{-1}. Column chromatography was performed on silica gel purchased from Sorbent Technologies (standard grade, 60 Å, 40–63 μm). Analytical thin layer chromatography (TLC) was performed on Whatman 250μm-thick silica gel 60 plates with a fluorescent indicator. Visualization of TLC spots was accomplished with UV light at 254 nm.

1.2. Procedures and spectral data

Synthesis of organic linkers **5a**–**5d** was started with Miyaura borylation of commercially available iodide **1**. The resulting pinacol borate **2** was then subjected to the two fold Suzuki coupling with dibromide **3a**–**3d** to give the corresponding dimethyl terphenyldicarboxylate derivatives **4a**–**4d**. The target linkers were obtained by saponification of **4a**–**4d** followed by, in the case of aniline derivative **5b**, thermolysis of the Boc protecting group. The procedure is summarized in Scheme S1.

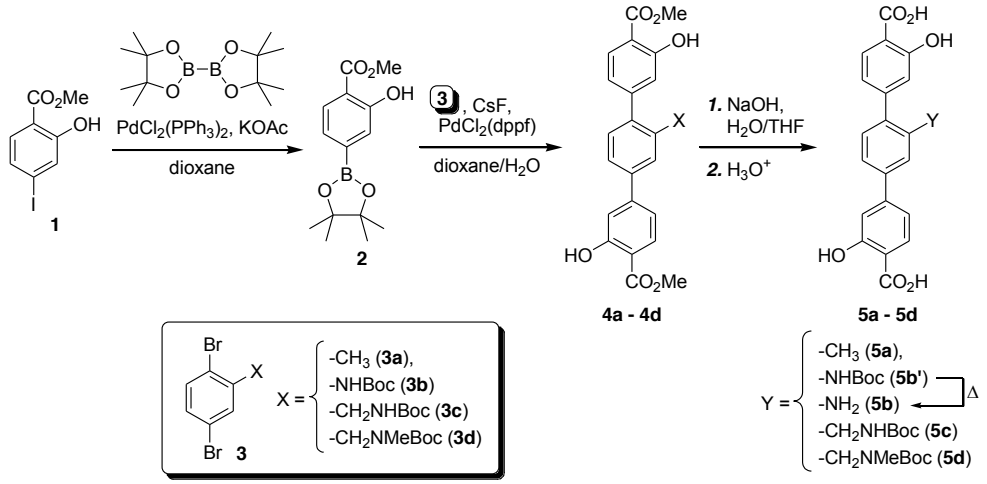

Scheme S1. Synthetic scheme of organic linkers **5a**–**5d**.

General procedure 1 (Suzuki–Miyaura coupling)

A *p*-dioxane/H_2O (2:1 v/v) mixture was deoxygenated by nitrogen bubbling for 30 min then added to a nitrogen-purged flask containing the required aryl dihalide **3** (1.0 relative mol amount), the boronic acid pinacol ester **2** (2.1 relative mol amount), CsF (6.0 relative mol amount), and $PdCl_2$(dppf) (2.5 mol% per halide). The resulting mixture was transferred to an oil bath preheated to 90 °C and stirred vigorously until completion of the reaction (progress periodically checked by TLC). After the reaction,

mixture was cooled down to room temperature; the corresponding coupling product was isolated as described per compound below.

General procedure 2 (saponification)

To a solution of the required ester (1.0 relative mol amount) in THF was added a solution of NaOH (10 relative mol amount) in H_2O to obtain a final concentration of 0.2 M for the ester (equal volumes of H_2O and THF). The resulting solution was stirred vigorously at 50 °C until the reaction completes (progress periodically checked by TLC). After cooled down to room temperature, THF was removed under vacuum to give typically slightly yellow solution. While being stirred, the aqueous layer was acidified with dilute HCl (1-3 M) and the resulting precipitate was collected by vacuum filtration, washed with ample H_2O, and dried in air for 24 h then in vacuo for 6 h to provide the corresponding hydrolysed product as typically a white powder.

3-Hydroxy-4-(methoxycarbonyl)phenylboronic acid pinacol ester (2).

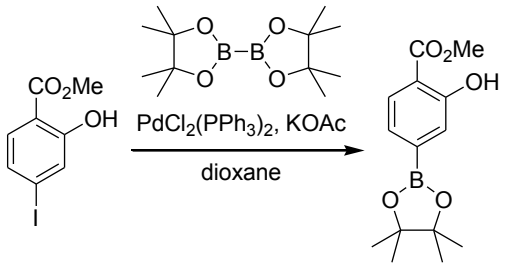

1 2

Scheme S2. Synthetic path for 3-hydroxy-4-(methoxycarbonyl)phenylboronic acid pinacol ester (**2**).

Dioxane (450 mL) was added to a flask containing iodide **1** (25.0 g, 90.0 mmol), bis(pinacolato)diboron (25.1 g, 98.8 mmol), KOAc (29.1 g, 297 mmol), and

$PdCl_2(PPh_3)_2$ (1.26 g, 1.80 mmol). The resulting suspension was deoxygenated by nitrogen bubbling at room temperature for 30 min, then immersed in oil bath preheated to 120 °C, and stirred at reflux for 16 h. After cooled down to room temperature, the mixture was filtered to remove the insoluble material using AcOEt to rinse the filter cake. The filtrate was evaporated to give brown oil which solidified slowly at room temperature. The crude product was purified by flash silica gel column chromatography (hexanes/AcOEt, 10:1) followed by recrystallization from hot hexanes to provide compound **2** as colorless crystals (20.3 g, 73.1 mmol, 81%). ^{1}H NMR (400 MHz, $CDCl_3$), [ppm]: 1.34 (s, 12H), 3.94 (s, 3H), 7.27 (d, J = 8.1 Hz, 1H), 7.41 (s, 1H), 7.80 (d, J = 7.9 Hz, 1H), 10.6 (s, 1H); ^{13}C{^{1}H} NMR (100 MHz, $CDCl_3$), [ppm]: 24.8, 52.3, 84.2, 114.2, 123.8, 124.7, 128.9, 160.7, 170.5; (Carbon directly bonded to boron was not observed). IR (ATR), $\bar{\nu}_{max}$ [cm^{-1}]: 3177 (br), 2982 (w), 1676 (m), 1619 (w), 1557 (w), 1502 (w), 1438(w), 1371 (sh), 1359 (s), 1329 (s), 1282 (m), 1220 (m), 1192 (m), 1169 (sh), 1136 (s), 1099 (s)961 (w), 920 (m), 850 (m), 821 (w), 788 (s), 712 (s), 638 (m), 663 (m), 562 (m), 547 (m), 500 (w), 467 (w).

^{t}Butyl-*N*-(2,5-dibromophenyl) carbamate (3b).[S1]

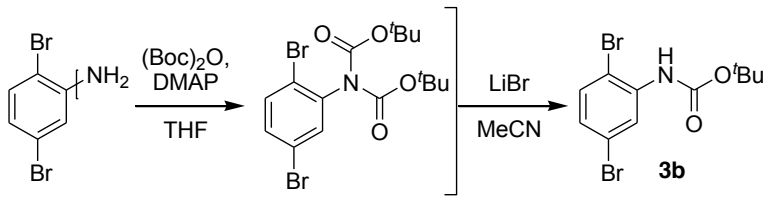

Scheme S3. Synthetic path for ^{t}butyl-*N*-(2,5-dibromophenyl) carbamate (**3b**).

2,5-Dibromoaniline (1.00 g, 3.99 mmol) was dissolved in THF (10 mL). After addition of di-^{t}butyl dicarbonate (2.60 g, 11.9 mmol) and 4-dimethylaminopyridine (49.1 mg, 0.402 mmol), the solution was stirred at 40 °C for 5 h. The reaction mixture

was cooled down to room temperature and evaporated to dryness to give brown oil. Acetonitrile (40 mL) and LiBr (1.07 g, 12.3 mmol) were added to the oil, and the resulting suspension was stirred at 65 °C for 8 h before cooled down to room temperature then evaporated to dryness. The crude product was subjected to flash silica gel column chromatography (hexanes/AcOEt, 20:1) to provide compound **3b** as a slightly yellow solid (1.24 g, 3.41 mmol, 85%). The material was subjected to the next step without further purification. ^{1}H NMR (400 MHz, $CDCl_3$), [ppm]: 1.53 (s, 9H), 6.99 (br s, 1H), 7.10 (dd, J = 8.5, 2.4 Hz, 1H), 7.33 (d, J = 8.5 Hz, 1H), 8.39 (d, J = 2.1 Hz, 1H);^{13}C{^{1}H} NMR (100 MHz, $CDCl_3$), [ppm]: 28.2, 81.6, 110.5, 122.0, 122.5, 126.6, 133.1, 137.4, 151.9. The NMR chemical shifts match the previously reported values.[S2]

^{t}Butyl-2,5-dibromobenzylcarbamate (3c)

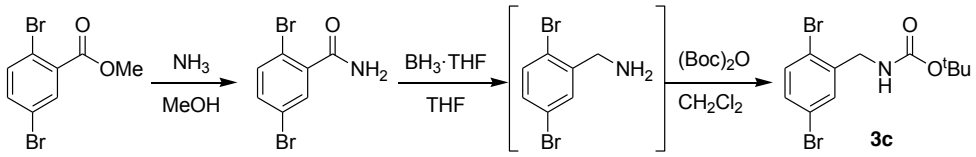

Scheme S4. Synthetic path for ^{t}butyl-2,5-dibromobenzylcarbamate (**3c**).

Methyl 2,5-dibromobenzoate (10.1 g, 34.4 mmol) was dissolved in 7 M NH_3 solution in methanol (100 mL) in air. The resulting solution was evenly separated to ten 20-mL scintillation vials, and stirred at room temperature for 20 h with the caps tightly closed. The reaction mixtures were combined and filtered to collect the white precipitate, which was then dispersed in hexanes (200 mL), recollected by filtration, and dried in vacuo to give 2,5-dibromobenzamide (9.44 g, 33.8 mmol, 98%). ^{1}H NMR (400 MHz, acetone-d_6), [ppm]: 7.04 (br s, 1H), 7.34 (br s, 1H), 7.51 (dd, J = 8.5, 2.4 Hz, 1H), 7.58

(d, J = 8.5 Hz, 1H), 7.62 (d, J = 2.4 Hz, 1H); $^{13}C\{^{1}H\}$ NMR (100 MHz, acetone-d_6), [ppm]: 118.8, 121.5, 132.4, 134.4, 135.8, 142.0, 168.2.

To a flask containing 2,5-dibromobenzamide (3.05 g, 10.9 mmol) was added 1 M BH_3 solution in THF (30 mL, 30 mmol), which was then stirred at reflux for 24 h before quenched by adding conc. HCl (3 mL). The solution was further refluxed for 2 h before cooled down to room temperature and basified to pH~10 by adding sat. Na_2CO_3. The reaction was partitioned between AcOEt (30 mL) and water (15 mL). The organic phase was isolated, and the aqueous phase was extracted with CH_2Cl_2 (3 × 30mL). The combined organic phase was dried over Na_2SO_4, filtered, and evaporated to give a light yellow liquid. The liquid was dissolved in CH_2Cl_2 (15 mL), to which di-^{t}butyl dicarbonate (2.65 mL, 11.5 mmol) was added. The solution was stirred for 2.5 h at room temperature, before addition of ethanolamine (0.33 mL). After further stirring at room temperature for 1 h, the reaction mixture was partitioned between CH_2Cl_2 (15 mL) and water (15 mL). The organic phase was isolated and the aqueous phase was extracted with CH_2Cl_2 (3 × 15 mL). The combined organic layer was dried over Na_2SO_4, filtered, and evaporated to give light yellow oil, which was purified by flash silica gel column chromatography (CH_2Cl_2/hexanes/AcOEt, 20:30:1). Compound **3c** was obtained as a white powder (2.55 g, 6.99 mmol, 64% from 2,5-dibromobenzoic acid). ^{1}H NMR (400 MHz, $CDCl_3$), [ppm]: 1.46 (s, 9H), 4.33 (d, J = 6.0 Hz, 2H), 5.06 (br s, 1H), 7.24 (dd, J = 8.4, 2.2 Hz, 1H), 7.38 (d, J = 8.4 Hz, 1H), 7.48 (d, J = 2.3 Hz, 1H); $^{13}C\{^{1}H\}$ NMR (100 MHz, $CDCl_3$), [ppm]: 28.3, 44.5, 80.0, 121.5, 121.8, 131.8, 132.1, 134.0, 140.0, 155.7; IR (ATR), $\bar{\nu}_{max}$ [cm^{-1}]: 3344 (m), 3086 (w), 3065 (w), 3009 (w), 2979 (w), 2971 (w), 2938 (w), 1682 (s), 1514 (s), 1461 (m), 1428 (m), 1392 (m), 1365 (m), 1303 (m), 1273 (s), 1251 (s), 1234 (m), 1195 (m), 1159 (s), 1083 (m), 1041 (w), 1026 (s), 930 (m),

918 (m), 886 (m), 851 (m), 811 (s), 784 (m), 768 (m), 726 (w), 611 (m), 547 (w), 511 (m), 459 (m), 443 (s).

^{t}Butyl-2,5-dibromobenzyl(methyl) carbamate (3d)

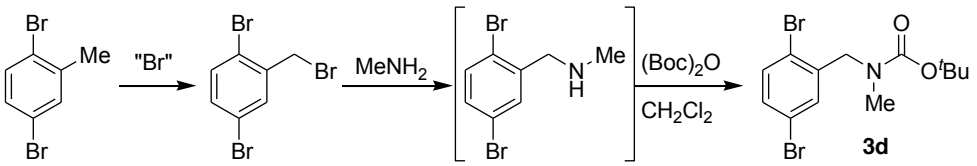

Scheme S5. Synthetic path for ^{t}butyl-2,5-dibromobenzyl(methyl) carbamate (**3d**).

N-Bromosuccinimide (1.78 g, 10.0 mmol) was added to a 200 mL two necked round bottom flask and the atmosphere was replaced from air into nitrogen. Anhydrous CH_2Cl_2 (80 mL) was then added to the flask and the solution was cooled down to 0 °C. Once the temperature was reached, $ZrCl_4$ (118 mg, 0.500 mmol) and 2,5-dibromotoluene (1.38 mL, 10.0 mmol) were added to the solution. The reaction was stirred 48 h from 0 °C to room temperature and then quenched by adding a saturated aqueous solution of $NaHCO_3$ (20 mL). The organic phase was separated and extracted with saturated aqueous NaCl solution (3 × 20 mL). The organic phase was dried over Na_2SO_4, filtered, and evaporated to give a brown / yellow liquid, which was purified by silica gel column chromatography (hexanes/CH_2Cl_2, 60:40). 2-(Bromomethyl)-1,4-dibromobenzene was obtained as a white powder (2.17 g, 6.60 mmol, 66% from 2,5-dibromotoluene). ^{1}H NMR (400 MHz, $CDCl_3$), [ppm]: 4.53 (s, 2H), 7.29 (dd, J = 8.5, 2.3 Hz, 1H), 7.43 (d, J = 8.5 Hz, 1H), 7.59 (d, J = 2.4 Hz, 1H). This intermediate was utilized in the next step without further purification.

To a 200 mL flask containing 2-(bromomethyl)-1,4-dibromobenzene (1.13 g, 3.40 mmol), were added 60 mL of THF and 1.8 mL of an aqueous methylamine solution (40

wt. %). The reaction was stirred at room temperature 18 h under nitrogen. The solvent was then removed under reduced pressure and the residue was partitioned in 110 mL of a mixture of CH_2Cl_2/15 wt. % $NaHCO_3$ in deionized water (60:50). The aqueous fraction was washed with CH_2Cl_2 (2 × 30 mL) and the organic fractions were collected, dried over anhydrous Na_2SO_4 and filtered. The solvent was evaporated under reduced pressure and the yellow oil was utilized in the next step without further purification.

The liquid was dissolved in CH_2Cl_2 (80 mL), to which di-^{t}butyl dicarbonate (1.48 mL, 6.42 mmol) was added. The solution was stirred for 18 h at room temperature and under nitrogen, before addition of ethanolamine (0.33 mL). After further stirring at room temperature for 3 h, the reaction mixture was partitioned between CH_2Cl_2 (15 mL) and water (15 mL). The organic phase was isolated and the aqueous phase was extracted with CH_2Cl_2 (3 × 15 mL). The combined organic layer was dried over Na_2SO_4, filtered, and evaporated to give light yellow oil, which was purified by flash silica gel column chromatography (CH_2Cl_2/AcOEt, 100:1). Compound **3d** was obtained as a white powder (1.15 g, 3.00 mmol, 88% from 2-(bromomethyl)-1,4-dibromobenzene). ^{1}H NMR (400 MHz, $CDCl_3$), [ppm]: 1.47 (d, J = 34.4 Hz, 9H), 2.90 (d, J = 20.1 Hz, 3H), 4.47 (d, J = 50.3 Hz, 2H), 7.26 (m, 2H), 7.48 (d, J = 8.3 Hz, 1H).

3,3''-Dihydroxy-2'-methyl-[1,1':4',1''-terphenyl]-4,4''-dicarboxylic acid (5a)

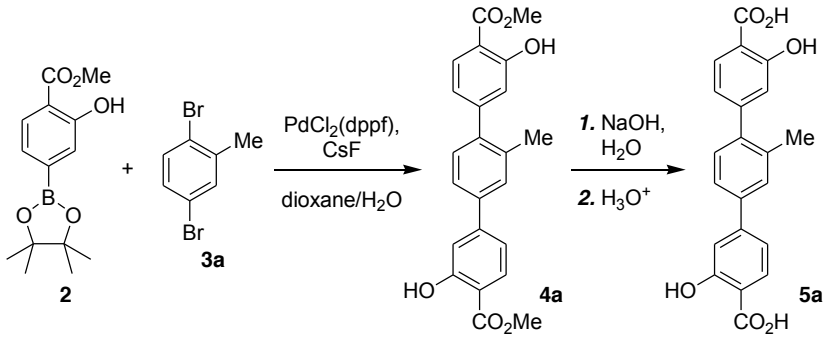

Scheme S6. Synthetic path for organic linker **5a**.

Boronate **2** (4.67 g, 16.8 mmol) and dibromide **3a** (1.10 mL, 7.98 mmol) were subjected to Suzuki–Miyaura coupling following General procedure 1. After cooled down to room temperature, the reaction mixture was partitioned between CH_2Cl_2 (300 mL) and 10% NH_4Cl (60 mL). The organic layer was isolated and the aqueous layer was extracted with CH_2Cl_2 (2 × 60 mL). The organic layers were combined, dried over Na_2SO_4, filtered, and evaporated in vacuo to provide a dark brown solid, which was then subjected to a filtration through a pad of silica gel (CH_2Cl_2). The filtrate was evaporated in vacuo and the resulting light yellow solid was recrystallized from hot toluene to provide **4a** as white needles (2.72 g, 6.94 mmol, 87%). ^{1}H NMR (500 MHz, $CDCl_3$), [ppm]: 2.35 (s, 3H), 3.98 and 3.99 (two s, 6H in total), 6.88 (dd, J = 6.9, 1.4 Hz, 1H), 6.99 (d, J = 1.3 Hz, 1H), 7.16 (dd, J = 8.2, 1.5 Hz, 1H), 7.25 (d, J = 1.4 Hz, 1H), 7.31 (d, J = 7.8 Hz, 1H), 7.50 (d, J = 7.9 Hz, 1H), 7.53 (s, 1H), 7.89 (d, J = 7.9 Hz, 1H), 7.90 (d, J = 8.1 Hz, 1H), 10.83 and 10.84 (two s, 2H in total); ^{13}C{^{1}H} NMR (126 MHz, $CDCl_3$), [ppm]: 20.5, 52.3, 52.3, 111.1, 111.2, 115.7, 118.1, 118.1, 120.4, 124.7, 129.3, 129.7, 129.9, 130.3, 135.8, 139.2, 140.8, 148.0, 149.1, 161.3, 161.8, 170.5.

Compound **4a** (2.43 g, 6.20 mmol) was hydrolyzed as described in "General procedure 2" using 3 M HCl for acidification to attain a pH<2. After drying, linker **5a** was obtained as an off-white powder (2.08 g, 5.71 mmol, 92%). ^{1}H NMR (400 MHz, DMSO-d_6), [ppm]: 2.32 (s, 3H), 6.72–6.74 (overlapping s and dd, J = 5.9, 1.5 Hz, 2H), 7.07–7.09 (two m, 2H), 7.27 (d, 7.9 Hz, 1H), 7.53 (dd, J = 7.9, 1.4 Hz, 1H), 7.60 (s, 1H), 7.79–7.83(two m, 2H);^{13}C{^{1}H} NMR (100 MHz, DMSO-d_6), [ppm]: 20.3, 114.1, 115.8, 116.6, 116.9, 118.2, 124.3, 128.8, 129.8, 130.0, 130.7, 135.3, 138.7, 140.6, 144.3, 145.6, 161.9, 162.4, 171.9;IR (ATR), $\bar{\nu}_{max}$ [cm^{-1}]: 3355 (br w), 3396 (br w), 3015 (w), 2944 (w), 2914 (w), 2859 (w), 1650 (m), 1621 (m), 1577 (s), 1515 (m), 1481 (m), 1435 (m), 1404 (m), 1358 (m), 1330 (m), 1291 (m), 1259 (m), 1206 (m), 1159 (m), 903 (m), 816

(m), 780 (s), 700 (m), 577 (m), 445 (w), 427 (w); MS (HR-ESI), *m*/*z* calcd. for $C_{21}H_{15}O_6$ $[M-H]^-$ 363.0869, found 363.0869.

2'-Amino-3,3''-dihydroxy-[1,1':4',1''-terphenyl]-4,4''-dicarboxylic acid (5b)

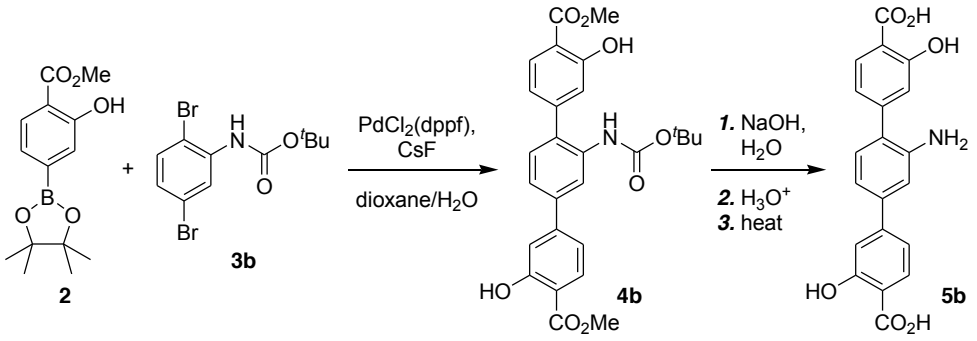

Scheme S7. Synthetic path for organic linker **5b**.

Boronate **2** (1.50 g, 5.39 mmol) and dibromide **3b** (0.901 g, 2.57 mmol) were subjected to Suzuki–Miyaura coupling by following General procedure 1. After cooled down to room temperature, the reaction mixture was partitioned between AcOEt (100 mL) and 10% NH_4Cl (50 mL). The organic layer was isolated and the aqueous layer was extracted with AcOEt (3 × 50 mL). The organic layers were combined, washed with brine (50 mL), dried over Na_2SO_4, filtered, and evaporated in vacuo to provide a dark grey solid, which was then subjected to flash silica gel chromatography [CH_2Cl_2, then CH_2Cl_2/AcOEt (50:1)]. The fractions containing compound **4b** were collected and evaporated in vacuo. The resulting light yellow solid was dissolved in hot toluene (10 mL) and the solution was cooled to room temperature to form white precipitates over a period of 40 min. Hexanes (10 mL) was added dropwise to form additional precipitate before the precipitate was collected by filtration then rinsed by toluene/hexanes (1:1, 40 mL) then hexanes (40 mL). The filtrate was evaporated and the resulting yellow solid was subjected to recrystallization in the same manner as above using 2 mL of toluene

and 2 mL of hexanes. The first and second crops were combined and dried under vacuum to provide compound **4b** as a white powder (1.04 g, 2.10 mmol, 82%). ^{1}H NMR (500 MHz, $CDCl_3$), [ppm]: 1.48 (s, 9H), 3.97 and 3.98 (two s, 6H in total), 6.59 (s, 1H), 6.92 (dd, *J* = 8.1, 1.5 Hz, 1H), 7.02 (d, *J* = 1.4 Hz, 1H), 7.20 (dd, *J* = 8.3, 1.6 Hz, 1H), 7.26 (d, *J* = 8.0 Hz, 1H), 7.27 (d, *J* = 1.5 Hz, 1H), 7.34 (dd, *J* = 8.0, 1.6 Hz, 1H), 7.87 (d, *J* = 8.2 Hz, 1H), 7.94 (d, *J* = 8.1 Hz, 1H), 8.44 (s, 1H), 10.81 (s, 1H), 10.90 (s, 1H); ^{13}C{^{1}H} NMR (126 MHz, $CDCl_3$), [ppm]: 28.2, 52.3, 52.4, 80.9, 111.3, 111.8, 115.8, 118.1, 118.3, 118.7, 120.0, 121.8, 130.0, 130.2, 130.2, 130.7, 135.6, 140.4, 145.5, 147.7, 152.6, 161.7, 161.9, 170.2, 170.4.

Compound **4b** (0.485 g, 0.983 mmol) was hydrolyzed as described in "General procedure 2" using 1 M HCl for acidification to attain a pH~6. After drying, the resulting white powder was heated under nitrogen at 180 °C for 2.5 h to remove *tert*-butyloxycarbonyl moieties to provide linker **5b** as a yellow powder (0.248 mg, 0.679 mmol, 69%). ^{1}H NMR (400 MHz, DMSO-d_6), [ppm]: 6.98 (dd, *J* = 8.0, 1.5 Hz, 1H), 7.03–7.05 (overlapping s and dd, 2H), 7.12–7.15 (overlapping peaks, 3H), 7.18 (dd, *J* = 8.3, 1.6 Hz, 1H), 7.85 and 7.87 (two s, 2H); ^{13}C{^{1}H} NMR (126 MHz, $CDCl_3$), [ppm]: 111.5, 111.9, 113.9, 114.4, 115.5, 116.7, 117.5, 119.7, 124.7, 130.6, 130.7, 130.8, 139.3, 145.6, 146.7, 147.4, 161.4, 161.4, 171.8, 171.8; IR (ATR), $\bar{\nu}_{max}$ [cm^{-1}]: 3349 (br w), 2991 (br m), 2848 (br m), 2554 (br w), 1652 (s), 1616 (s), 1561 (m), 1483 (m), 1451 (s), 1433 (s), 1347 (m), 1259 (s), 1228 (s), 1201 (s), 1161 (s), 1100 (m), 1022 (w), 964 (m), 904 (m), 861 (m), 806 (w), 774 (s), 693 (m), 671 (m), 651 (w), 637 (w), 594 (w), 578 (w), 539 (w), 517 (w), 495 (w), 478 (w), 447 (w); MS (HR-ESI), *m*/*z* calcd. for $C_{20}H_{14}NO_6$ $[M-H]^-$ 364.0821, found 364.0822.

Table S1. Crystal data and structure refinement for organic linker **5b** (-NH_2, Figure 1)

Identification code	Organic linker **5b** (-NH_2)
Empirical formula	$C_{24}H_{27}NO_8S_2$
Formula weight	521.58
Temperature/K	150.15
Crystal system	triclinic
Space group	*P*-1
a/Å	7.9219(4)
b/Å	10.4568(6)
c/Å	16.3932(8)
α/°	100.8525(15)
β/°	95.5763(18)
γ/°	110.9964(16)
Volume/Å^3	1224.90(11)
Z	2
ρ_{calc}mg/mm^3	1.414
μ/mm^{-1}	0.267
F(000)	548.0
Crystal size/mm^3	0.15 × 0.05 × 0.08
Radiation	MoKα (λ = 0.71073)
2Θ range for data collection	4.448 to 55.064
Index ranges	$-10 \le h \le 9$, $-12 \le k \le 13$, $-21 \le l \le 20$
Reflections collected	43051
Independent reflections	5580 [R_{int} = 0.0348, R_{sigma} = 0.0204]
Data/restraints/parameters	5580/0/423
Goodness-of-fit on F^2	1.057
Final *R* indexes [I>2σ (I)]	R_1 = 0.0406, wR_2 = 0.1004
Final *R* indexes [all data]	R_1 = 0.0521, wR_2 = 0.1091
Largest diff. peak/hole / e Å^{-3}	0.53/-0.33

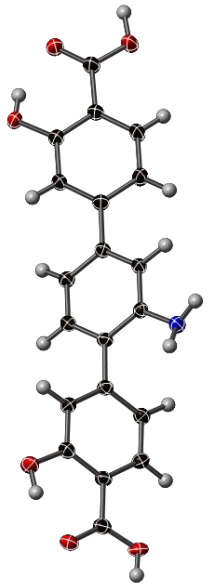

Figure S1. ORTEP representation of the amino-functionalized organic linker (-NH_2, linker **5d**, Figure 1) with 50% of probability. Color code: C (black), O (red), N (blue), and H (grey).

2'-(((*tert*-Butoxycarbonyl)amino)methyl)-3,3''-dihydroxy-[1,1':4',1''-terphenyl]-4,4''-dicarboxylic acid (5c)

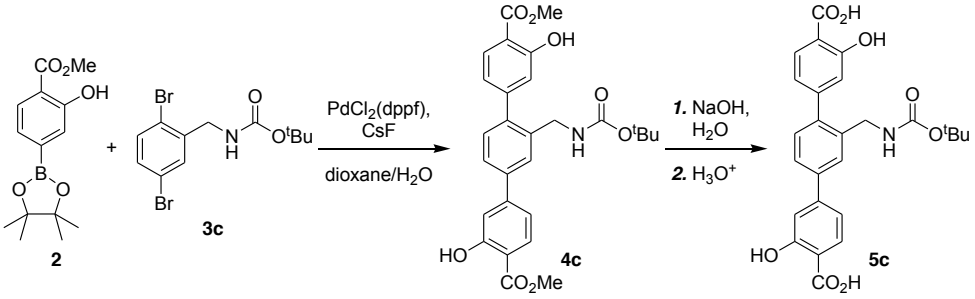

Scheme S8. Synthetic path for organic linker **5c**.

Boronate **2** (3.20 g, 11.5 mmol) and dibromide **3c** (2.01 g, 5.51 mmol) were subjected to Suzuki–Miyaura coupling by following General procedure 1. After cooled down to room temperature, the reaction mixture was partitioned between AcOEt (200

mL) and 10% NH_4Cl (50 mL). The organic layer was isolated and the aqueous layer was extracted with AcOEt (3×25 mL). The organic layers were combined, washed with brine (50 mL), dried over Na_2SO_4, filtered, and evaporated in vacuo to provide a black solid, which was then subjected to flash silica gel chromatography [CH_2Cl_2, thenCH_2Cl_2/AcOEt (50:1)]. The fractions containing compound **4c** were collected and evaporated in vacuo. The resulting light yellow solid was dissolved in toluene (20 mL), to which hexanes (20 mL) was added dropwise to form a white precipitate. The precipitate was collected by filtration, rinsed with toluene/hexanes (1:1, 10 mL), then dried in vacuo to provide pure **4c** as a white powder (2.14 g, 4.21 mmol, 76%). ^{1}H NMR (400 MHz, $CDCl_3$), [ppm]: 1.42 (s, 9H), 3.97 (s, 6H), 4.33 (d, *J* = 3.5 Hz, 2H), 4.79 (s, 1H), 6.85 (d, *J* = 7.8 Hz, 1H), 6.94 (s, 1H), 7.14 (d, *J* = 7.9 Hz, 1H), 7.29 (s, 1H), 7.29 (d, *J* = 7.7 Hz, 1H), 7.55 (d, *J* = 7.3 Hz, 1H), 7.68 (s, 1H), 7.87–7.90 (two overlapping d, 2H), 10.82 and 10.84 (two s, 2H); ^{13}C{^{1}H} NMR (100 MHz, $CDCl_3$), [ppm]: 28.3, 42.3, 52.3, 52.3, 79.6, 111.4, 111.4, 115.7, 117.9, 118.0, 120.2, 126.0, 127.0, 129.9, 130.2, 130.3, 136.6, 139.6, 140.2, 147.6, 147.9, 155.7, 161.4, 161.8, 170.3, 170.4.

Compound **4c** (2.10 g, 4.15 mmol) was hydrolyzed as described in "General procedure 2" to provide linker **5c** as an off-white powder (1.88 g, 3.92 mmol, 95%). ^{1}H NMR (500 MHz, DMSO-d_6), [ppm]: 1.20 and 1.37 (two s, 9H), 4.16 (d, *J* = 5.9 Hz, 2H), 6.94 (d, *J* = 8.3 Hz, 1H), 6.96 (s, 1H), 7.25 and 7.27 (overlapping s and d, 2H), 7.33 (d, *J* = 8.0 Hz, 1H), 7.49 (t, *J* = 5.9 Hz, 1H), 7.68 (d, *J* = 7.9 Hz, 1H), 7.85 (d, *J* = 8.0 Hz, 1H), 7.90 (d, *J* = 8.7 Hz, 1H); ^{13}C{^{1}H} NMR (126 MHz, DMSO-d_6), [ppm]: 28.3, 41.3, 78.0, 112.1, 112.3, 114.7, 117.5, 117.6, 120.3, 125.4, 126.2, 130.1, 130.3, 131.1, 137.7, 138.3, 139.5, 146.7, 147.2, 155.8, 161.0, 161.6, 171.9; IR (ATR), $\bar{\nu}_{max}$ [cm^{-1}]: 3400–2700 (br w), 2976 (w), 2931 (w), 2871 (w), 2567 (w), 1659 (s), 1619 (s), 1563 (m),

1500 (m), 1480 (m), 1454 (m), 1434 (m), 1394 (w), 1366 (m), 1340 (m), 1251 (s), 1202 (s), 1158 (s), 1097 (m), 1046 (w), 1027 (w), 905 (m), 875 (m), 844 (w), 816 (m), 778 (s), 692 (m), 595 (w), 569 (w), 510 (w), 456 (w); MS (HR-ESI), *m*/*z* calcd. for $C_{26}H_{24}NO_8$ $[M-H]^-$ 478.1502, found 478.1499.

2'-(((*tert*-Butoxycarbonyl)(methyl)amino)methyl)-3,3''-dihydroxy-[1,1':4',1''-terphenyl]-4,4''-dicarboxylic acid (5d)

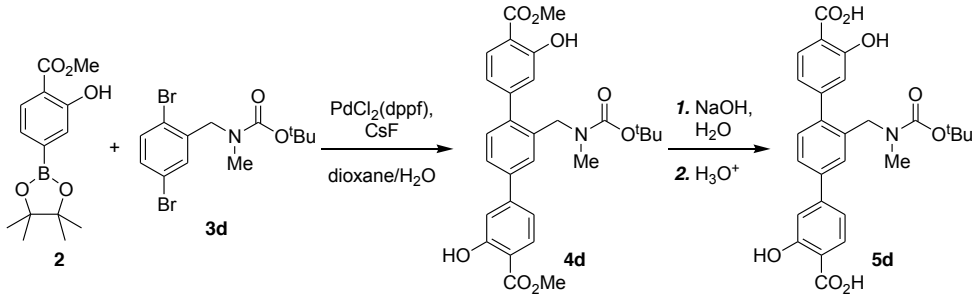

Scheme S9. Synthetic path for organic linker **5d**.

Boronate **2** (1.2 g, 4.3 mmol) and dibromide **3d** (0.80 g, 2.1 mmol) were subjected to Suzuki–Miyaura coupling following general procedure 1. After cooled down to room temperature, the reaction mixture was partitioned between CH_2Cl_2 (300 mL) and 10% NH_4Cl (60 mL). The organic layer was isolated and the aqueous layer was extracted with CH_2Cl_2 (2 × 60 mL). The organic layers were combined, dried over Na_2SO_4, filtered, and evaporated in vacuo to provide a dark brown solid, which was then subjected to a filtration through a pad of silica gel (CH_2Cl_2). The filtrate was evaporated in vacuo and the resulting light yellow solid was subjected to flash silica gel chromatography [hexanes/AcOEt (90:10)]. Solvent evaporation in vacuo to provide pure **4d** as a white powder (1.0 g, 1.9 mmol, 90%). ^{1}H NMR (400 MHz, $CDCl_3$), [ppm]: 1.45 (d, J = 19.7 Hz, 9H), 2.72 (d, J = 29.3 Hz, 3H), 3.98 (s, 6H), 4.48 (d, J = 24.4 Hz,

2H), 6.83 (d, *J* = 6.9 Hz, 1H), 6.94 (s, 1H), 7.13 (d, *J* = 8.0 Hz, 1H), 7.23, (s, 1H), 7.31 (d, *J* = 7.9 Hz, 1H), 7.55 (m, 2H), 7.90 (m, 2H), 10.83 (s, 2H).

Compound **4d** (0.98 g, 1.9 mmol) was hydrolyzed as described in general procedure 2. After drying, linker **5d** was obtained as an off-white powder (0.83 g, 1.7 mmol, 90%). ^{1}H NMR (400 MHz, $CDCl_3$), [ppm]: 1.31 (d, *J* = 42.2, 9H), 2.65 (s, 3H), 4.44 (s, 2H), 6.90 (m, 2H), 7.23 (m, 2H), 7.35 (d, *J* = 7.9 Hz, 1H), 7.52 (s, 1H), 7.70 (dd, *J* = 7.9, 1.7 Hz, 1H), 7.87 (m, 2H); ^{13}C{^{1}H} NMR (126 MHz, $CDCl_3$), [ppm]: 27.90, 34.36, 54.90, 78.78, 112.16, 112,27, 114.63, 117.25, 117.51, 119.99, 125.68, 130.28, 131.04, 138.48, 146,54, 147.04, 160.90, 161.55, 171.72, 171.77. IR (ATR), $\bar{\nu}_{max}$ [cm^{-1}]: 3400–2700 (br w), 2986 (w), 2933 (w), 2857 (w), 2560 (w), 1657 (s), 1641 (s), 1564 (m), 1500 (m), 1482 (m), 1454 (s), 1420 (m), 1321 (m), 1315 (m), 1256 (s), 1210 (s), 1149 (s), 910 (m), 901 (m), 822 (m), 782 (s), 694 (m), 602 (w), 570 (w), 508 (m), 448 (w), 424 (w); MS (HR-ESI), *m*/*z* calcd. for $C_{27}H_{26}NO_8$ $[M-H]^-$ 492.1658, found 492.1655.

Table S2. Crystal data and structure refinement for organic linker **5d** (-CH_2NMeBoc, Figure 1)

Identification code	Organic linker **5d** (-CH_2NMeBoc)
Empirical formula	$C_{54}H_{54}N_2O_{16}$
Formula weight	986.99
Temperature/K	150.15
Crystal system	monoclinic
Space group	$P2_1/n$
a/Å	5.5232(2)
b/Å	11.0315(3)
c/Å	39.7408(12)
α/°	90
β/°	93.570(2)
γ/°	90
Volume/Å^3	2416.68(13)
Z	2
ρ_{calc}mg/mm^3	1.356
μ/mm^{-1}	0.836
F(000)	1040.0
Crystal size/mm^3	0.1 × 0.04 × 0.04
Radiation	CuKα (λ = 1.54178)
2Θ range for data collection	8.318 to 129.802°
Index ranges	$-6 \le h \le 5$, $-12 \le k \le 12$, $-45 \le l \le 46$
Reflections collected	15905
Independent reflections	3992 [R_{int} = 0.0447, R_{sigma} = 0.0374]
Data/restraints/parameters	3992/0/429
Goodness-of-fit on F^2	1.059
Final R indexes [I>2σ (I)]	R_1 = 0.0479, wR_2 = 0.1086
Final R indexes [all data]	R_1 = 0.0710, wR_2 = 0.1201
Largest diff. peak/hole / e Å^{-3}	0.29/-0.26

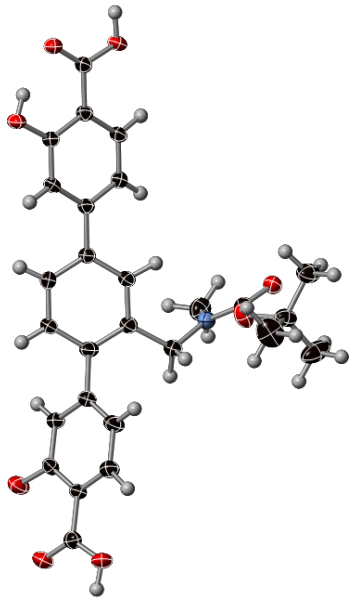

Figure S2. ORTEP representation of the secondary amine-functionalized organic linker (-CH_2NMeBoc, linker **5d**, Figure 1) with 50% of probability. Color code: C (black), O (red), N (blue), and H (grey).

2. Synthesis of metal-organic frameworks (MOFs)

2.1. General

Functionalized IRMOF-74-III compounds were prepared according to the procedure reported in literature.[S3] $Mg(NO_3)_2 \cdot 6H_2O$ (160 mg, 0.62 mmol) and the organic linker (0.188 mmol) were added into a 20-mL scintillation vials and dissolved with 15 mL of DMF. The vial was sonicated for 10 minutes and 1.0 mL of methanol followed by 1.0 mL of deionized water, were added to this solution. The vial was sonicated again for 10 minutes and the sealed vial with the resulting clear solutions, was placed into an isothermal oven at 120 °C for 20 h. After cooling down to room temperature, the solution was removed by syringe and the solid was immersed in 10 mL of DMF for 3 h. The liquid was then decanted and process repeated three times per day for 3 days. This whole protocol was repeated with methanol during 2 days to obtain the solid with washed interior. The solvent within the pores of the resulting solid was removed under dynamic vacuum initially at room temperature and then by heating at 120 °C for 8 h. The guest free samples were analyzed by PXRD and their surface area was determined by nitrogen adsorption experiments.

2.2. Procedures

IRMOF-74-III-CH_3: The synthesis was performed according to general procedure **2.1**, yielding 90% of white crystals (Figure S3a). PXRD was collected on activated sample (guest free). The high degree of correspondence between the sample pattern and that of the simulated model indicates that the bulk material has the same crystal structure as the predicted by simulation (Figure S10, Section 5). To determine the presence of functional groups in the MOF pores, we have performed ^1H NMR of digested samples in 50 mM DCl in a DMSO-d_6/D_2O mixture (Figure S4, Section 4).

The resonance peak at 2.31 ppm (s, 3H) confirms the presence of -CH_3 functional group in the framework. IR (ATR), $\bar{\nu}_{max}$ [cm^{-1}]: 2022 (w), 1983 (w), 1670 (m), 1598 (m), 1581 (s), 1433 (s) 1394 (m), 1367 (m), 1323 (m) 1257 (m), 1218 (m), 1157(w), 1108 (w), 927 (m), 877 (w), 827 (m), 795 (m), 701 (w), 608 (m) 580 (m).

IRMOF-74-III-NH_2: Due to the lower solubility of the organic linker in comparison with other linkers reported here, the procedure for this MOF synthesis was slightly modified. $Mg(NO_3)_2 \cdot 6H_2O$ (160 mg, 0.62 mmol) and the organic linker **5b** (68.7 mg, 0.188 mmol) were added into a 20-mL scintillation vials and dissolved with 15 mL of DMF. The vial was sonicated for 10 minutes and 2.5 mL of methanol followed by 2.5 mL of deionized water were added to this solution. The vial was sonicated again for 10 minutes and the sealed vial with the resulting clear solutions, was placed into an isothermal oven at 120 °C for 20 h. Yellow crystals were obtained in 84% reaction yield (Figure S3b). PXRD was collected on activated sample (guest free). The high degree of correspondence between the sample pattern and that of the simulated model indicates that the bulk material has the same crystal structure as the predicted by simulation (Figure S11, Section 5). To determine the presence of functional groups in the MOF pores, we have performed ^1H NMR of digested samples in 50 mM DCl in a DMSO-d_6/D_2O mixture (Figure S5, Section 4). The absence of aliphatic signals and the correspondence of the aromatic proton integrals confirm the presence of -NH_2 functional group in the framework. IR (ATR), $\bar{\nu}_{max}$ [cm^{-1}]: 3330 (br w), 3027 (br w), 1608 (s), 1577 (s), 1524 (m), 1440 (s) 1418 (s), 1372 (m), 1219 (m) 930 (m), 793 (m), 709 (m), 610 (m).

IRMOF-74-III-CH_2NHBoc: The synthesis was realized according to the general procedure above, yielding 81% of pale yellow crystals (Figure S3c). PXRD was collected on activated sample (guest free). The high degree of correspondence between the sample pattern and that of the simulated model indicates that the bulk material has the same crystal structure as the predicted by simulation (Figure S12, Section 5). To determine the presence of functional groups in the MOF pores, we have performed ^1H NMR of digested samples in 50 mM DCl in a DMSO-d_6/D_2O mixture (Figure S6, Section 4). The resonance peaks at 1.35 ppm (d, 9H) and 4.14 ppm (s, 2H) corresponding to the Boc protecting group and benzyl amine (-CH_2-) respectively; confirm the presence of -CH_2NHBoc functional group in the framework. IR (ATR), $\bar{\nu}_{max}$ [cm^{-1}]: 3360 (br w), 2979 (w), 1692 (s), 1585 (s), 1516 (m), 1433 (s) 1372 (s), 1250 (w), 1219 (m) 1159 (m), 1045 (w), 922 (m), 892 (w), 831 (m), 793 (m), 709 (m), 610 (m).

IRMOF-74-III-$CH_2NMeBoc$: The synthesis was realized according to the general procedure above, yielding 81% of pale yellow crystals (Figure S3e). PXRD was collected on activated sample (guest free). The high degree of correspondence between the sample pattern and that of the simulated model indicates that the bulk material has the same crystal structure as the predicted by simulation (Figure S13, Section 5). To determine the presence of functional groups in the MOF pores, we have performed ^1H NMR of digested samples in 50 mM DCl in a DMSO-d_6/D_2O mixture (Figure S7, Section 4). The resonance peaks at 1.27 ppm (d, 9H), 2.63 ppm (s, 3H) and 4.42 ppm (s, 2H) corresponding to the Boc protecting group, *N*-CH_3 and benzyl amine -CH_2- respectively; confirm the presence of -$CH_2NMeBoc$ functional group in the framework. IR (ATR), $\bar{\nu}_{max}$ [cm^{-1}]: 3360 (br w), 2979 (m), 2926 (m), 1661 (m), 1600 (sh), 1577 (s),

1432 (s), 1402 (m) 1372 (m), 1257 (m), 1218 (m) 1151 (m), 967 (w), 930 (m), 876 (w), 830 (m), 792 (m), 709 (m), 571 (w).

3. Thermal post-synthetic Boc deprotection.

3.1. General

The functionalized IRMOF-74-III crystals were subjected to solvent washing procedure described in section 2.1. The compounds were transferred using a glass pipette into a 10 mL reaction tube containing 3 mL of 2-ethyl-1-hexanol, 150 μL of ethylene glycol and 150 μL of deionized water. The heterogeneous mixture was subjected to 230 °C microwave heating for 10 minutes. The mixture was allowed to cool down to room temperature and the DMF and methanol solvent washing procedure was repeated. The obtained microcrystalline samples were analyzed by PXRD and ^{1}HNMR after digestion.

3.2. Procedures

IRMOF-74-III-CH_2NH_2: The Boc protecting group was removed by microwave heating as described above. The yellow crystals of IRMOF-74-III-CH_2NH_2 were recovered in 98% reaction yield (Figure S3d). PXRD was collected on activated sample (guest free). The high degree of correspondence between the sample pattern and that of the sample before the deprotection procedure indicates that the bulk material remains crystalline and with the same underlying topology after the post-synthetic deprotection (Figure S14, Section 5). The successful Boc-deprotection was confirmed by the absence of the Boc resonance peak at 1.35 ppm in the ^{1}H NMR of digested samples in 50 mM DCl in a DMSO-d_6/D_2O mixture (Figure S8, Section 4). IR (ATR), $\bar{\nu}_{max}$ [cm^{-1}]: 3024 (br w), 2940 (w), 1607 (sh), 1584 (s), 1516 (sh), 1440 (s) 1402 (sh), 1371 (s), 1325 (m), 1264 (w), 1219 (m), 1158 (w), 967 (w), 929 (m), 884 (w), 837 (m), 792 (m), 708 (m), 610 (m), 571 (w).

IRMOF-74-III-CH_2NHMe: The Boc group was removed by microwave heating as described above. The strong yellow crystals of IRMOF-74-III-CH_2NHMe were recovered in 94% reaction yield (Figure S3f). PXRD was collected on activated sample (guest free). The high degree of correspondence between the sample pattern and that of the sample before the deprotection procedure indicates that the bulk material remains crystalline and with the same underlying topology after the post-synthetic deprotection (Figure S15, Section 5). The successful Boc-deprotection was confirmed by the absence of the Boc resonance peak at 1.27 ppm in the ^1H NMR of digested samples in 50 mM DCl in a DMSO-d_6/D_2O mixture (Figure S9, Section 4). IR (ATR), $\bar{\nu}_{max}$ [cm^{-1}]: 3064 (br w), 1608 (m), 1585 (s), 1524 (sh), 1440 (s) 1410 (m), 1372 (m), 1326 (w), 1257 (w), 1219 (m), 1151 (w), 978 (w), 922 (m), 884 (w), 831 (m), 793 (m), 709 (m), 610 (m), 572 (w).

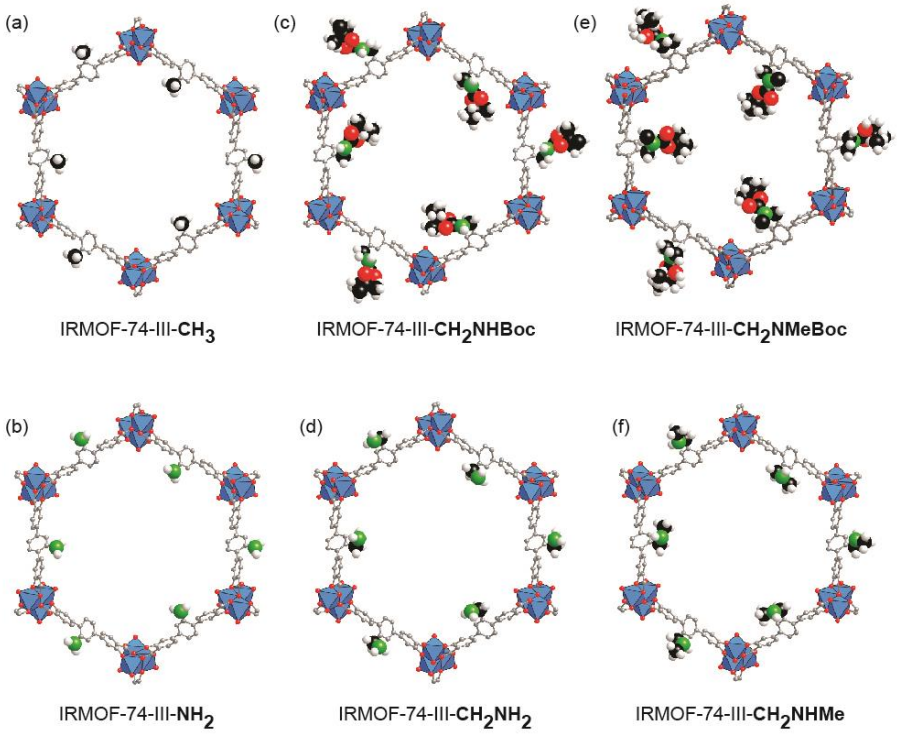

Figure S3. Structure of the six functionalized IRMOF-74-III synthesized in this work. (a) IRMOF-74-III-CH_3, (b) -NH_2, (c) -CH_2NHBoc, (d) -CH_2NH_2, (e) -$CH_2NMeBoc$, and (f) -CH_2NHMe. The introduced functionalities are highlighted using space filing model. Color code: C in black, H in white, O in red, and N in green. In the framework C atoms are shown in grey, O in red, and Mg as blue polyhedra.

4. Solution ^{1}H NMR of digested samples

4.1. General Procedure.

Typically, for the digestion of the MOF samples; ~10 mg of functionalized IRMOF-74-III were dried in air 12 h after solvent washing with DMF and methanol. Then 0.5 mL of DMSO-d_6 and 10 μL of mM DCl in D_2O (35 wt. %), were added. The suspension was sonicated 1 min and left at room temperature until clear solution was obtained. The ^{1}H NMR spectra were recorded immediately after (~10 min).

4.2. Characterization of functionalized IRMOF-74-III

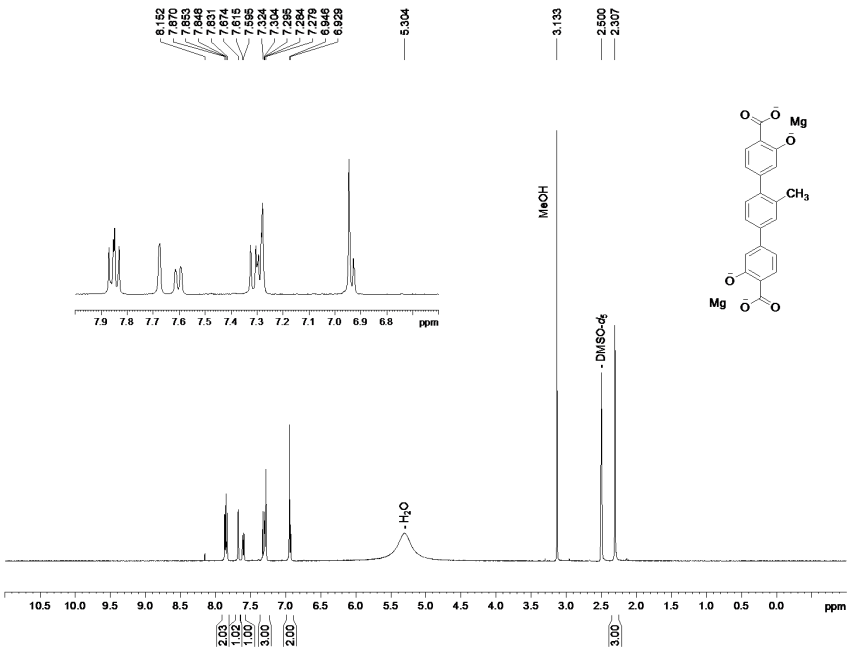

Figure S4. ^{1}H NMR spectra of IRMOF-74-III-CH_3 digested sample in 50 mM DCl/DMSO-d_6/D_2O mixture. Inset, expanded aromatic region in the spectra.

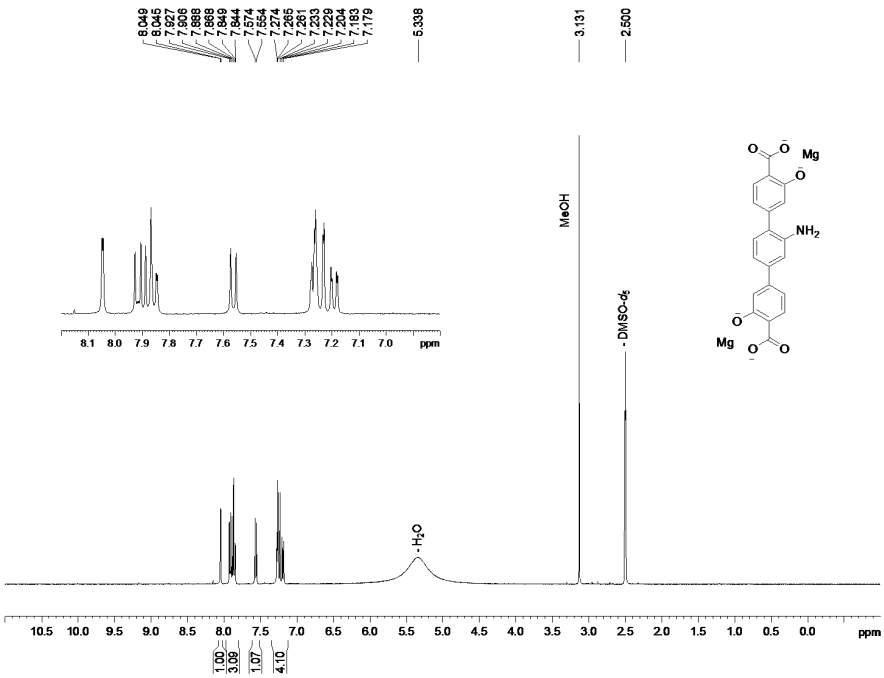

Figure S5. ^{1}H NMR spectra of IRMOF-74-III-NH_2 digested sample in 50 mM DCl/DMSO-d_6/D_2O mixture. Inset, expanded aromatic region in the spectra.

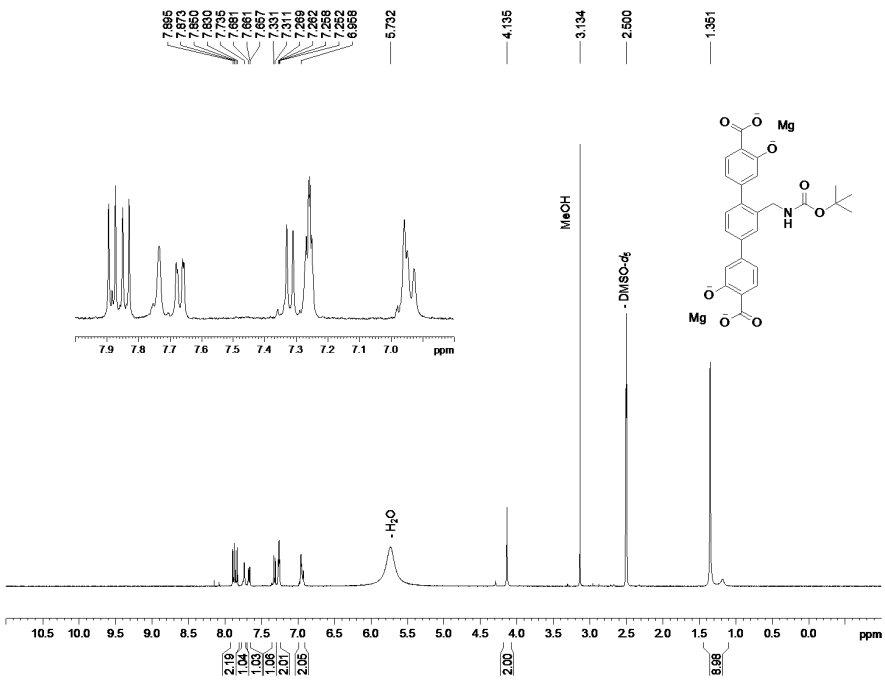

Figure S6. ^{1}H NMR spectra of IRMOF-74-III-CH_2NHBoc digested sample in 50 mM DCl/DMSO-d_6/D_2O mixture. Inset, expanded aromatic region in the spectra.

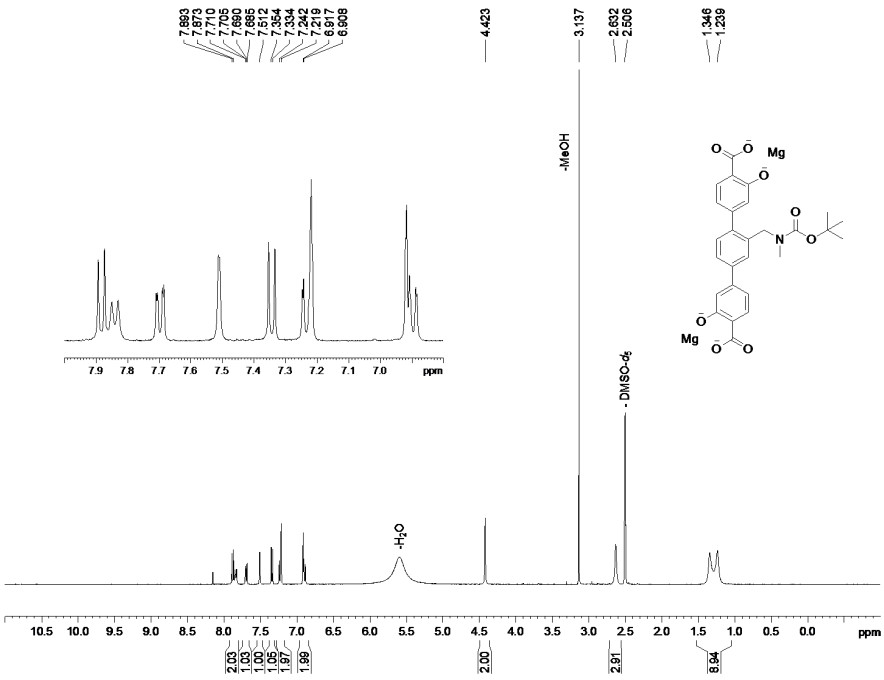

Figure S7. ^{1}H NMR of IRMOF-74-III-CH_2NMeBoc digested sample in 50 mM DCl/DMSO-d_6/D_2O mixture. Inset, expanded aromatic region in the spectra.

4.3 Characterization of functionalized IRMOF-74-III after post-synthetic deprotection of the Boc groups.

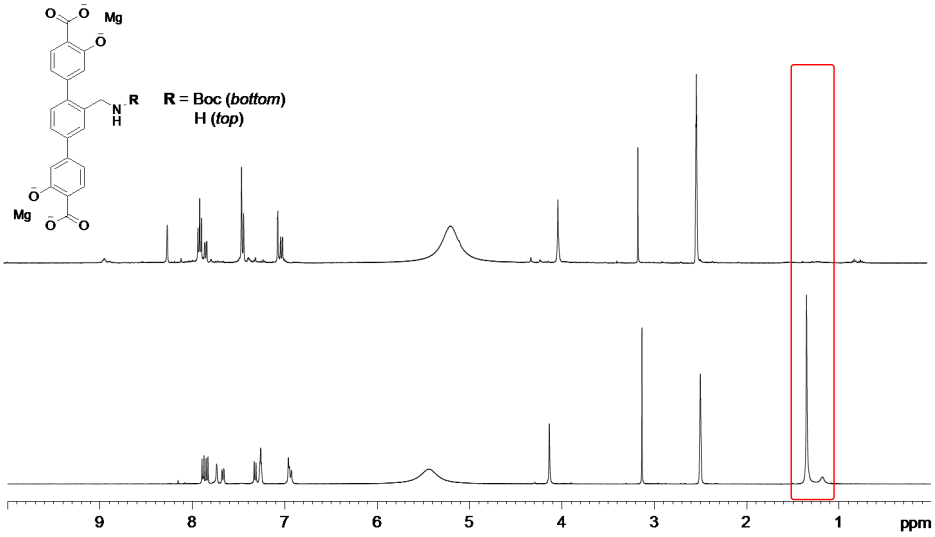

Figure S8. Comparison of ^{1}H NMR spectra for digested primary amine functionalized IRMOF-74-III samples in 50 mM DCl/DMSO-d_6/D_2O mixture: IRMOF-74-III-CH_2NHBoc (bottom) and IRMOF-74-III-CH_2NHBoc (top); before and after microwave deprotection respectively.

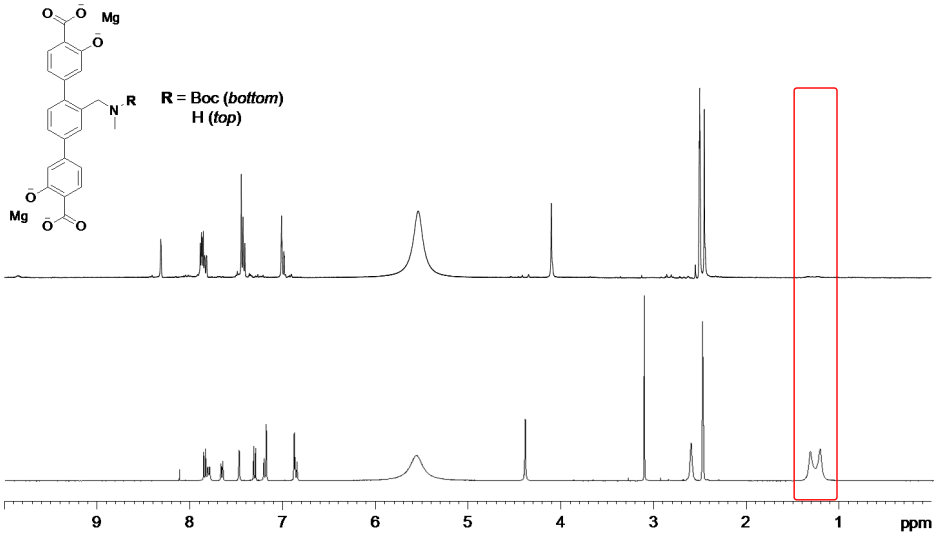

Figure S9. Comparison of ^{1}H NMR spectra for digested secondary amine functionalized IRMOF-74-III samples in 50 mM DCl/DMSO-d_6/D_2O mixture: IRMOF-74-III-CH_2NMeBoc (bottom) and IRMOF-74-III-CH_2NHMe (top); before and after microwave deprotection respectively.

5. Powder X-Ray Diffraction (PXRD) Characterization

5.1. Synthesis of functionalized IRMOF-74-III

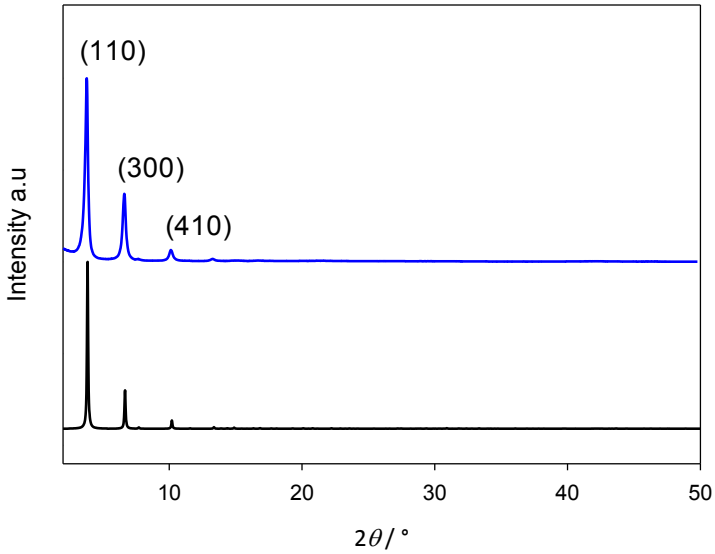

Figure S10. PXRD pattern of as-prepared IRMOF-74-III-CH_3 (blue) and calculated pattern for IRMOF-74-III (black).

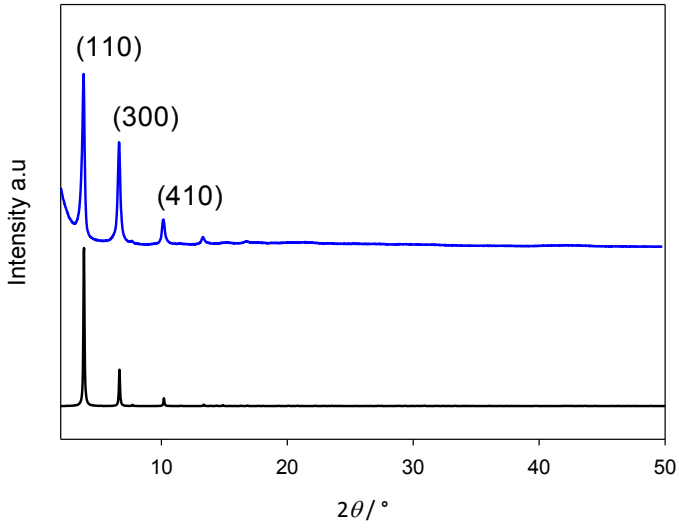

Figure S11. PXRD pattern of as-prepared IRMOF-74-III-NH_2 (blue) and calculated pattern for IRMOF-74-III (black).

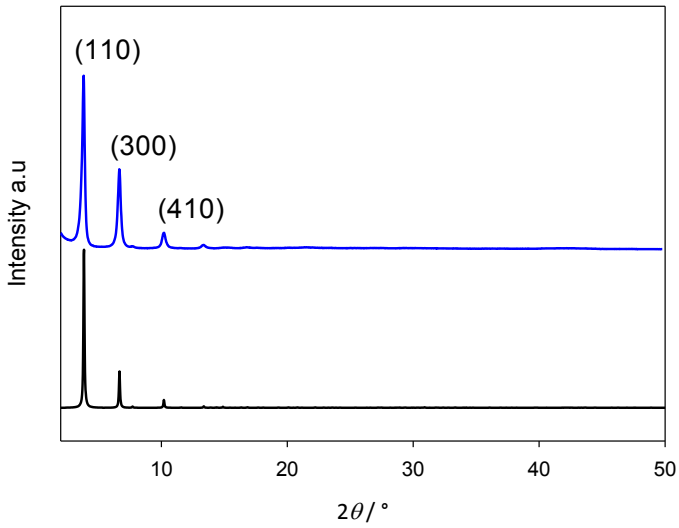

Figure S12. PXRD pattern of as-prepared IRMOF-74-III-CH_2NHBoc (blue) and calculated pattern for IRMOF-74-III (black).

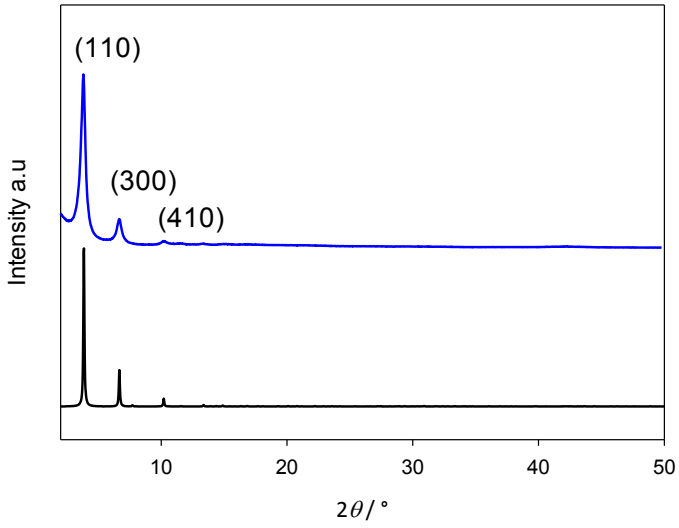

Figure S13. PXRD pattern of as-prepared IRMOF-74-III-$CH_2NMeBoc$ (blue) and calculated pattern for IRMOF-74-III (black).

5.2. Thermal post-synthetic deprotections of Boc group

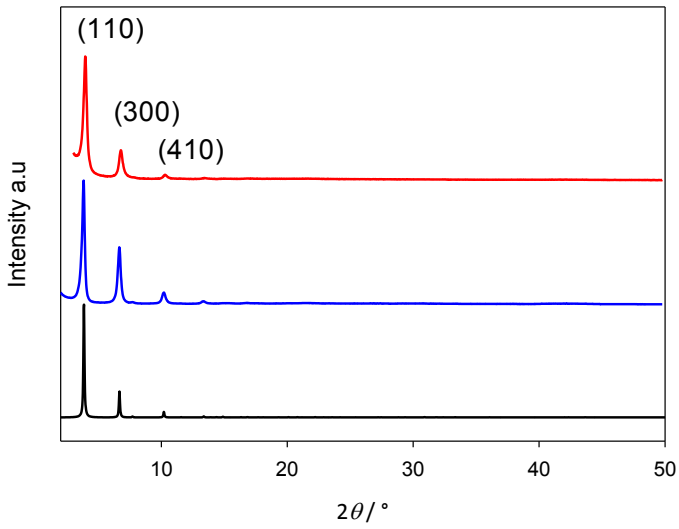

Figure S14. PXRD patterns of IRMOF-74-III-CH_2NH_2 (red) and IRMOF-74-III-CH_2NHBoc (blue). Calculated pattern for IRMOF-74-III (black) was overlaid.

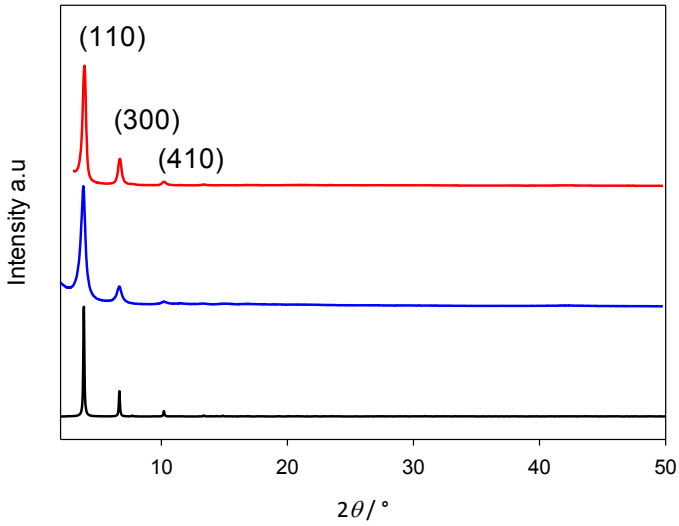

Figure S15. PXRD patterns of IRMOF-74-III-CH_2NHMe (red) and IRMOF-74-III-$CH_2NMeBoc$ (blue). Calculated pattern for IRMOF-74-III (black) was overlaid.

5.3. PXRD Characterization of the IRMOF-74-III-CH_2NH_2 before and after breakthrough experiments

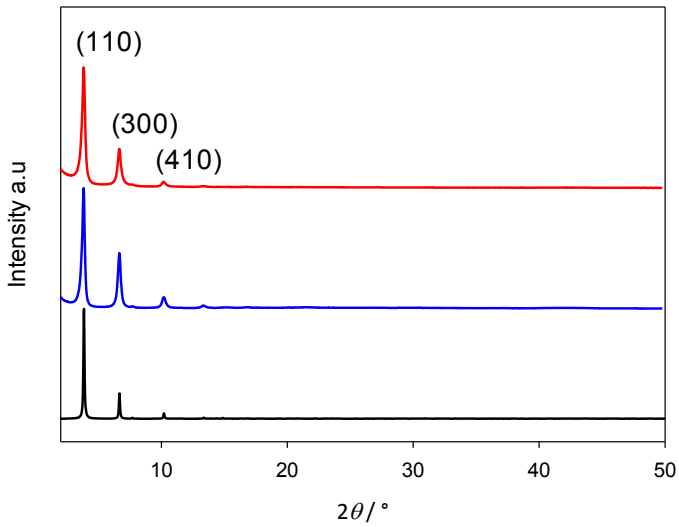

Figure S16. PXRD patterns of IRMOF-74-III-CH_2NH_2 before (blue) and after (red) the breakthrough experiments in the presence of water. Calculated pattern for IRMOF-74-III (black) was overlaid for comparison.

6. Nitrogen adsorption measurements

BET surface area reflects the geometrical surface of MOF materials; therefore, bulky functionalities may create more accessible surface. In addition to the differences found during the activations conditions, we cannot fully exclude the possibility that the part of the MOF structure was damaged during the deprotection process since MOF samples after post-synthetic modification reactions sometimes show a H4 type hysteresis loop[S4] attributed to intercrystalline voids in the sample.[S5] As such, surface areas may not be necessarily related to the size of the functional group present in the pores of IRMOF-74-III.

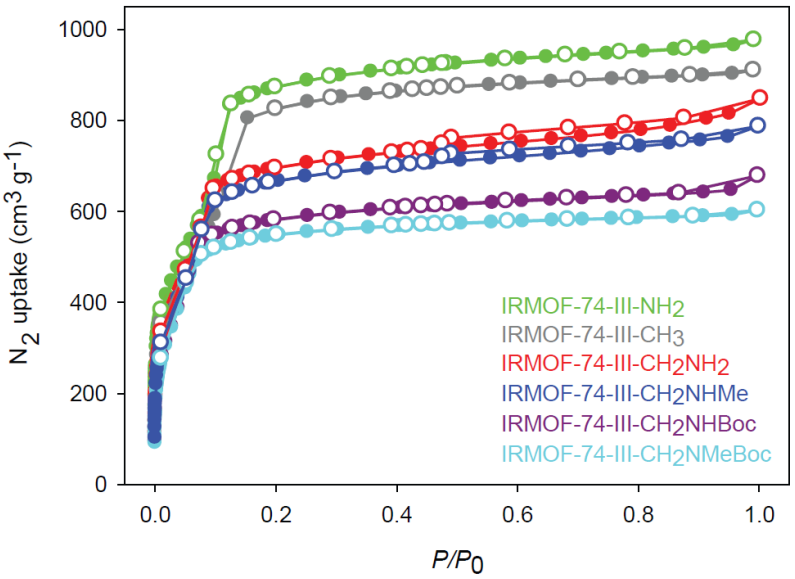

Figure S17. Nitrogen adsorption isotherms for functionalized IRMOF-74-III measured at 77 K. IRMOF-74-III-CH_3 (blue), IRMOF-74-III-NH_2 (pink), IRMOF-74-III-CH_2NHBoc (purple), IRMOF-74-III-CH_2NH_2 (red), IRMOF-74-III-$CH_2NMeBoc$ (cyan), and IRMOF-74-III-CH_2NHMe (green).

Table S3. Summary of pore volumes and surface areas for the series of IRMOF-74-III presented in this work.

IRMOF-74-III	Pore Volume ($cm^3\ g^{-1}$)	BET ($m^2\ g^{-1}$)	Langmuir ($m^2\ g^{-1}$)
-CH_3	1.37	2640	3940
-NH_2	1.44	2720	4130
-CH_2NHBoc	0.95	2170	2720
-CH_2NH_2	1.14	2310	3270
-$CH_2NMeBoc$	0.89	2220	2540
-CH_2NHMe	1.13	2250	3150

7. Carbon dioxide uptake capacities

To prepare guest free form of IRMOF-74-III-CH_2NH_2, we employed the same (and modified) activation procedures of IRMOF-74-III-CH_3. However, digestion NMR spectra of activated IRMOF-74-III-CH_2NH_2 showed presence of small amounts of solvent molecules (larger amount of water compared to the Boc protected compounds, presumably due to the use of water as solvent for the Boc deprotection procedure). This observation implies that these solvent molecules remained in the MOF even after the activation procedure. Due to the employed activation conditions (120 °C and vacuum) it is reasonable to think that the solvent molecules were occupying strong binding sites in the MOF, such as metal coordination sites. Therefore, unlike in IRMOF-74-III-CH_3, open magnesium sites are not available in IRMOF-74-III-CH_2NH_2. This explains why IRMOF-74-III-CH_2NH_2 did not show a significant improvement compared to IRMOF-74-III-CH_3 at 760 Torr, even when new chemisorption sites were created by the introduction of amine functionalities in IRMOF-74-III-CH_3.

The total carbon dioxide uptake should be the sum of the uptake at the open magnesium sites and at the chemisorptions sites. If all open metal sites in IRMOF-74-III-CH_3 are fully occupied by carbon dioxide at 760 Torr and 25 °C, expected uptake based only on the magnesium sites is ca. 100 $cm^3\ g^{-1}$. Similarly if all amine functionalities in IRMOF-74-III-CH_2NH_2 form carbamates, expected carbon dioxide uptake based only on the chemisorption sites is ca. 50 $cm^3\ g^{-1}$.

Table S4. Summary of carbon dioxide uptake capacities at 800 Torr and 25 °C for the series of IRMOF-74-III presented in this work.

IRMOF-74-III	CO_2 uptake ($cm^3\ g^{-1}$)	CO_2 uptake (mol f.u.$^{-1}$)[a]
-CH_3	66.1	1.2
-NH_2	71.0	1.3
-CH_2NHBoc	46.7	1.1
-CH_2NH_2	73.2	1.4
-$CH_2NMeBoc$	42.7	1.0
-CH_2NHMe	63.9	1.2

[a] f.u. corresponds to formula unit [Mg_2(linker)] which does not include coordinated solvent to the magnesium sites.

8. Solid-state NMR

8.1. General

High resolution solid-state NMR spectra were recorded at ambient temperature on a Tecmag Discovery spectrometer using a Doty magic angle spinning (MAS) probe with 4 mm (outside diameter) zirconia rotors. Cross-polarization with MAS (CP/MAS) was used to acquire ^{13}C data at 75.47 MHz. Standard inversion recovery experiments were performed on the ^{1}H channel to determine the adequate recycle delay (1.6 seconds). A ramped-amplitude cross-polarization matching condition was used with the center of the increasing proton ramp saddled around the full breadth of the first matching sideband condition above the center band. The center band matching frequency was 48 kHz, the MAS rate was 10 kHz, and the CP contact time was 5 milliseconds. Continuous wave (CW) decoupling was applied during acquisition at a frequency of 35 kHz. The ^{13}C chemical shifts are given relative to the methylene carbon signal of adamantane assigned to 37.77 ppm as a secondary reference. 1024 transients were recorded and processed with 25 Hz of exponential line broadening.

8.2. Spectroscopic evidence for the formation of carbamic species

IRMOF-74-III-NH_2, -CH_2NHBoc, -CH_2NH_2, and -CH_2NHMe samples (~ 70 mg) were activated as described in the report and transferred into a 20-mL scintillation vial in a globe box under Ar. The Ar was removed from the vial under reduced pressure (100 mTorr) and replaced with 1 bar of ^{13}C-labeled carbon dioxide (Sigma-Aldrich, 99 atom % ^{13}C; <3 atom % ^{18}O). The sample was exposed to ^{13}C-labeled carbon dioxide for one day and transferred to zirconia NMR rotors right before the NMR measurement.

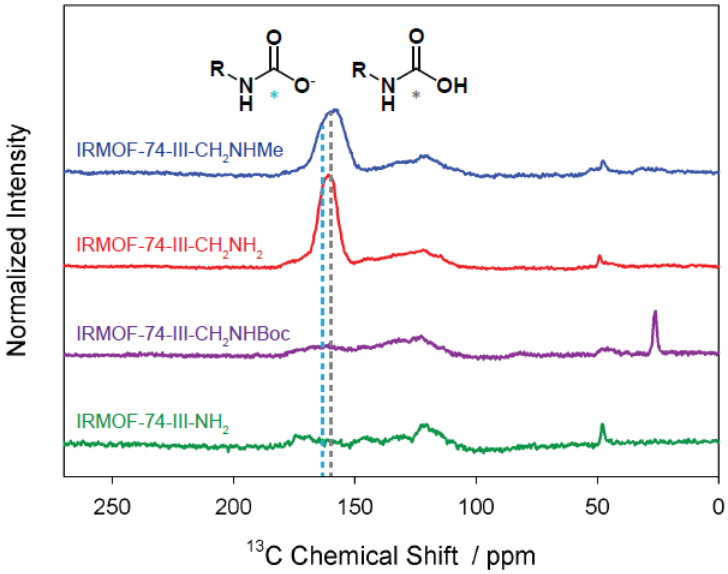

Figure S18. ^{13}C CP/MAS spectra of IRMOF-74-III-NH_2 (green), -CH_2NHBoc, -CH_2NH_2 (purple), -CH_2NHMe (red), and IRMOF-74-III-CH_2NH_2 (blue) treated with ^{13}C-labeled carbon dioxide and recorded at 25 °C. The last two samples show a resonance peak centered at δ = 160 ppm, ascribed to carbamamic acid and an overlapped peak at δ = 164 ppm corresponding to carbamate ions. The observed signals at δ = 48 ppm in all spectra correspond to DMF in the MOF pores, while the observed resonance peak at δ = 26 ppm for IRMOF-74-III-CH_2NHBoc (purple) is attributed to the Boc protecting group (^{t}butyl group). The peak width in the CP/MAS ^{13}C NMR spectra can be attributed to the magic angle offset, as well as the overlapping of carbamic acid and carbamate resonances.

9. Breakthrough experiments

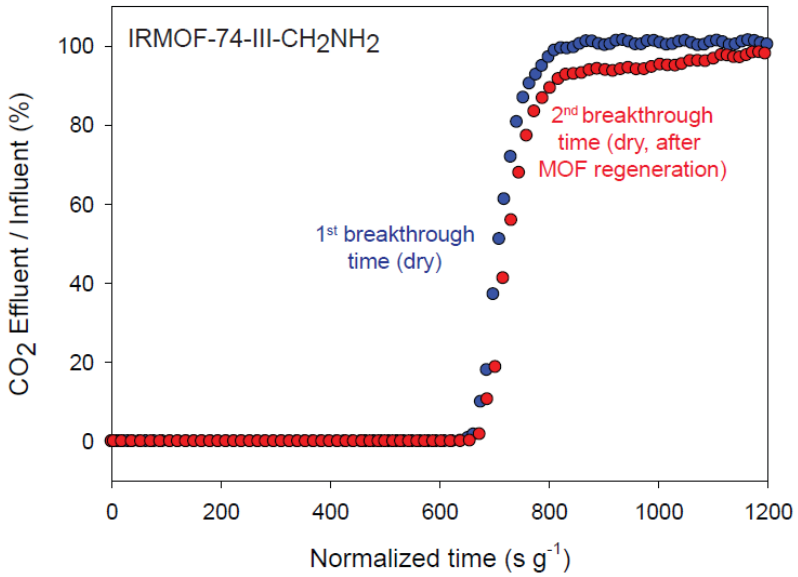

Figure S19. Breakthrough curves for IRMOF-74-III-CH_2NH_2 under dry conditions. First and second cycles (sample after regeneration by heating at 95 °C for 30 min) are shown in blue and red respectively.

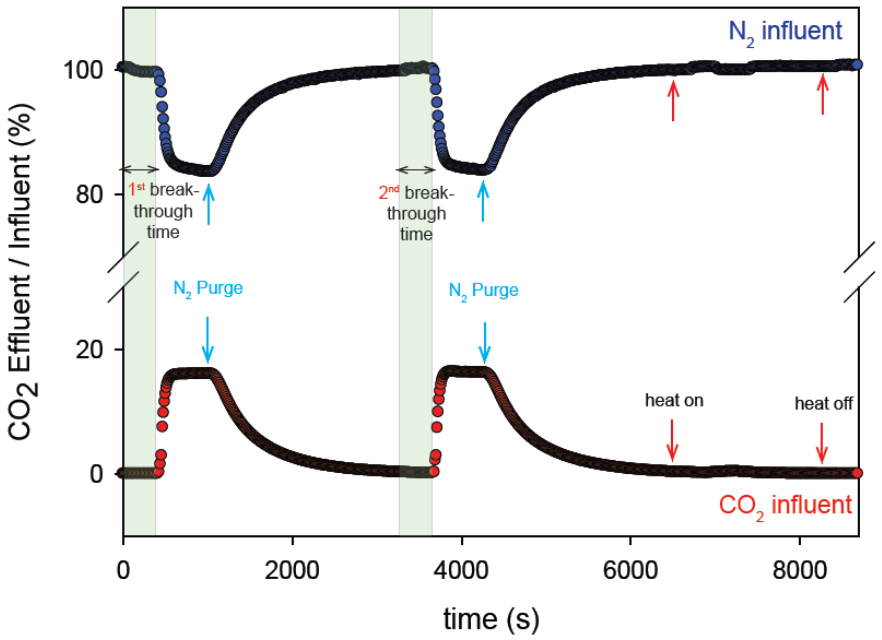

Figure S20. Breakthrough curves under dry conditions for IRMOF-74-III-CH_3. The breakthrough times for each cycle, has been highlighted as light green area (1^{st} and 2^{nd} breakthrough time for 1^{st} and 2^{nd} cycles, respectively). Nearly 5 times longer desorption time under dry nitrogen flow, compare to those for IRMOF-74-III-CH_3NH_2 (Figure 3a in the main text), indicates that carbon dioxide molecules are tightly bound to the Mg open metal site. The second breakthrough times, after nitrogen purge, was found to be nearly equal to the first (1380 ± 10 s g^{-1} and 1440 ± 10 s g^{-1} for the first and second breakthrough times respectively) and no carbon dioxide signal was observed upon heating indicating the absence of chemisorption process.

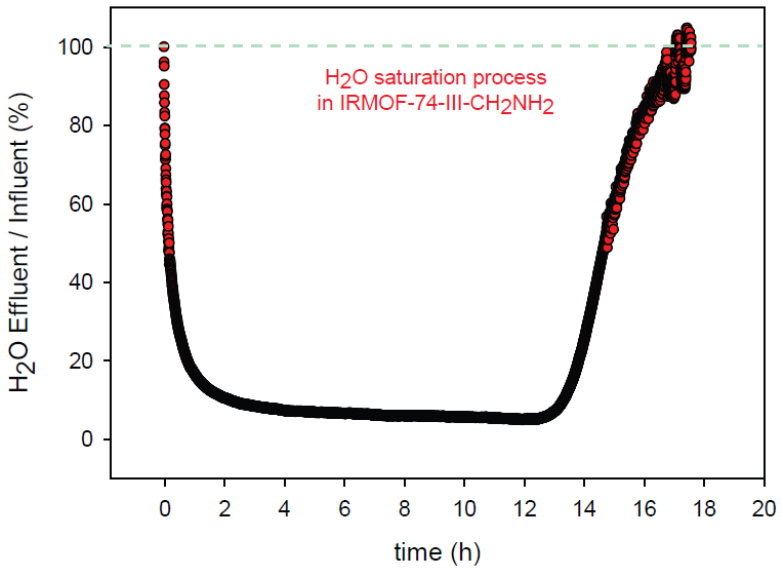

Figure S21. Time course of the percent composition of water in the wet nitrogen stream (65% relative humidity). The adsorbent bed contains activated IRMOF-74-III-CH_2NH_2.

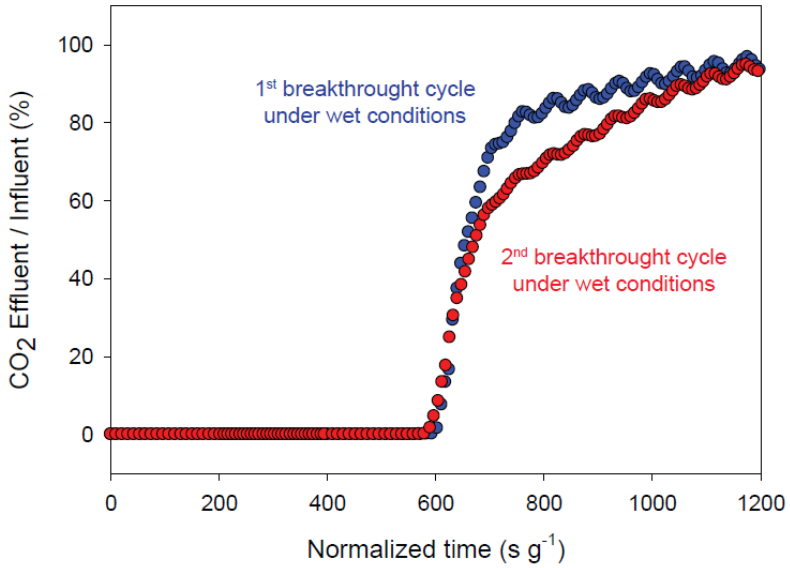

Figure S22. Breakthrough curves of IRMOF-74-III-CH_2NH_2 in the presence of water after vapor saturation (i.e. first cycle, blue) and after recovery of the material by passing through nitrogen and heating at 90 °C for 30 minutes (second cycle, red). The breakthrough times are nearly identical.

It should be noted that carbon dioxide show high solubility in water; therefore the amount of carbon dioxide that can be absorbed in the pore under the presence of water is also estimated. The solubility of carbon dioxide under the breakthrough conditions [i.e. 120 Torr (partial pressure) and 25 °C] is about 0.1 cm^3 (STP) per gram of water (i.e. 0.008 mol%).[S6] Although we do not know the adsorbed amount of water in the pore, it should be less than the pore volume of MOF materials at 65% RH. Therefore, the amount of carbon dioxide absorbed in water is much smaller than that chemisorbed (> 10 cm^3 g^{-1}).

10. Complete References 4 (b), 5 (g), and 9

(4) (b) Nugent, P.; Belmabkhout, Y.; Burd, S. D.; Cairns, A. J.; Luebke, R.; Forrest, K.; Pham, T.; Ma, S.; Space, B.; Wojtas, L.; Eddaoudi, M.; Zaworotko, M. J. *Nature* **2013**, *495*, 80.

(5) (g) Li, B.; Zhang, Z.; Li, Y.; Yao, K.; Zhu, Y.; Deng, Z.; Yang, F.; Zhou, X.; Li, G., Wu, H.; Nijem, N.; Chabal, Y. J.; Lai, Z.; Han, Y.; Shi, Z.; Feng, S.; Li J. *Angew*. *Chem*. *Int*. *Ed*. **2012**, *51*, 1412.

(9) Deng, H.; Grunder, S.; Cordova, K., Valente, C.; Furukawa, H.; Hmadeh, M.; Gándara, F.; Whalley, A. C.; Liu, Z.; Asahina, S.; Kazumori, H.; O'Keeffe, M.; Terasaki, O.; Stoddart, J. F.; Yaghi O. M. *Science* **2012**, *336*, 1018.

11. References

(S1) Hernández, J. N.; Ramírez, M. A.; Martín, V. *J*. *Org*. *Chem*. **2003**, *68*, 743.

(S2) Durban, M. M.; Kazarinoff, P. D.; Segawa, Y; Luscombe, C. K. *Macromolecules* **2011**, *44*, 4721.

(S3) Deng, H.; Grunder, S., Cordova, K. E.; Valente, C.; Furukawa, H.; Hmadeh, H.; Gándara, F.; Whalley, A. C.; Liu, Z.; Asahina, S.; Kazumori, H.; O'Keeffe, M.; Terasaki, O.; Stoddart, J. F.; Yaghi, O. M. *Science* **2012**, *336*, 1018.

(S4) Doonan, C. J.; Morris, W.; Furukawa, H.; Yaghi O. M. *J*. *Am*. *Chem*. *Soc*. **2009**, *131*, 9492.

(S5) Vishnyakov, A.; Ravikovitch, P. I.; Neimark, A. V.; Bülow, M.; Wang, Q. M. *Nano Lett*. **2003**, *3*, 713.

(S6) Carroll, J. J.; Slupsky, J. D.; Mather, A. E. *J*. *Phys*. *Chem*. *Ref*. *Data* **1991**, *20*, 1201.